

REPORT DOCUMENTATION PAGE

Form Approved
OMB No. 074-0188

Public reporting burden for this collection of information is estimated to average 1 hour per response, including the time for reviewing instructions, searching existing data sources, gathering and maintaining the data needed, and completing and reviewing this collection of information. Send comments regarding this burden estimate or any other aspect of this collection of information, including suggestions for reducing this burden to Washington Headquarters Services, Directorate for Information Operations and Reports, 1215 Jefferson Davis Highway, Suite 1204, Arlington, VA 22202-4302, and to the Office of Management and Budget, Paperwork Reduction Project (0704-0188), Washington, DC 20503

1. AGENCY USE ONLY (Leave blank) 2. REPORT DATE **08/24/00** 3. REPORT TYPE AND DATES **Final 4/01/96-12/31/99**

4. TITLE AND SUBTITLE

Agile Optical Phased Arrays for Microspacecraft

5. FUNDING NUMBERS

F49620-96-1-0206

6. AUTHOR(S)

Richard L. Fork

7. PERFORMING ORGANIZATION NAME(S) AND ADDRESS(ES)

**University of Alabama in
Huntsville
301 Sparkman Drive
Huntsville, AL 35899**

8. PERFORMING ORGANIZATION REPORT NUMBER

9. SPONSORING / MONITORING AGENCY NAME(S) AND ADDRESS(ES)

**AFOSR, Dr. H. Schlossberg,
TEL 703 696-7549**

10. SPONSORING / MONITORING AGENCY REPORT NUMBER

11. SUPPLEMENTARY NOTES

12a. DISTRIBUTION / AVAILABILITY STATEMENT

**DISTRIBUTION STATEMENT A
Approved for Public Release
Distribution Unlimited**

20010312 102

13. ABSTRACT

Means of steering high power optical beams by means of compact low mass technology suitable for spacecraft and microspacecraft were addressed. Non-mechanical means were sought that permit redirection of the beam over half space in times of the order of 1 microsecond or less. The effort included means for steering of optical pulses as well as continuous optical beams. The large apertures needed in space applications and the interest in structures having minimum mass and volume required attention to thin film structures with rapid switching capability that could produce large group delay in a compact structure. Mechanisms for both group delay and phase delay control were examined. New technology was identified in the form of a novel microresonator based switching element employing photonic band structures. The technology explored appears consistent with extrapolation to high average power, e.g., multi-megawatts. The work examined double clad optical fiber as the amplifying element, but also initiated an examination of a novel class of free space amplifiers. A microsatellite was launched and placed in orbit, but a telemetry problem prevented active acquisition of data from the satellite.

14. SUBJECT TERMS **Optical phased arrays, optical switch, group delay**

15. NUMBER OF PAGES **62**

16. PRICE CODE

17. SECURITY CLASSIFICATION OF REPORT

None

18. SECURITY CLASSIFICATION OF THIS PAGE

None

19. SECURITY CLASSIFICATION OF ABSTRACT

None

20. LIMITATION OF ABSTRACT **None**

DISTRIBUTION STATEMENT AUTHORIZATION RECORD

Title: Agile Optical Phased Arrays for
Microspacecraft

Authorizing Official: H. Schlossberg

Agency: AFOSR Ph. No. (703) 696-7549

☐ Internet Document: URL: _____
(DTIC-OCA Use Only)

Distribution Statement: (Authorized by the source above.)

- ☒ A: Approved for public release, distribution unlimited.
- ☐ B: U. S. Government agencies only. (Fill in reason and date applied). Other requests shall be referred to (Insert controlling office).
- ☐ C: U. S. Government agencies and their contractors. (Fill in reason and date applied). Other requests shall be referred to (Insert controlling office).
- ☐ D: DoD and DoD contractors only. (Fill in reason and date applied). Other requests shall be referred to (Insert controlling office).
- ☐ E: DoD components only. (Fill in reason and date applied). Other requests shall be referred to (Insert controlling office).
- ☐ F: Further dissemination only as directed by (Insert controlling DoD office and date), or higher authority.
- ☐ X: U. S. Government agencies and private individuals or enterprises eligible to obtain export-controlled technical data in accordance with DoD Directive 5230.25.

NOTES: _____

J. Keith
DTIC Point of Contact

14 MAR 2001
Date

1. Objectives: The objectives were to identify and develop compact low mass means for rapid non-mechanical steering of high power optical beams in space. A primary objective was designing and testing technology capable of supporting a system having average power >1 kW, agile steering (microsecond or less time constants), and time resolved signals (e.g., duration <150 fsec). Additional objectives were thin film based technology, low overall mass, and designs that show traceability to steering of high peak power pulsed optical beams. While the level of support did not allow addressing of high average power exploration of high peak power conditions was sought.

2. Approach: Design, calculation, simulation and experimental work were used to explore thin film photonic band structures for controlling the group delay and phase delay of short optical pulses. An experimental facility was created for generating optical pulses, amplifying those pulses, and converting those monochromatic pulses to white light continuum pulses. Additional instrumentation was added to enable the use of those pulses to measure the influence of specific photonic band structures on those pulses with special attention to the femtosecond metrology of the transmission and group delay. Simulation capabilities were also developed that enabled the modeling of photonic switching elements for control of group and phase delay.

3. Accomplishments/New Findings: Results were obtained in four different areas:

- 1) Simulations and design of a single photonic element were developed and used as a guide for fabrication of several different photonic elements. The later photonic elements included means for electronically varying the optical properties of the element
- 2) An experimental facility was built, made operational, and used to measure the properties of the photonic control elements. Measurements were obtained simultaneously of the device transmission, and temporal modification of a short optical pulse with a temporal resolution of a few femtoseconds over a bandwidth of the order of 50 nm. This bandwidth permitted simultaneous examination of the device behavior over multiple photonic resonances.
- 3) Simulations, but no experiments, were used to explore the properties of the novel switch constructed from three separate photonic elements arranged in a particular configuration for switching in support of true time delay. The switch addressed the problem of providing large adjustable group delay in a thin layered photonic structure. The device and its properties are described in Section 6.
- 4) A micro-satellite was built and launched. Details of the satellite effort are given in Section 7. The micro-satellite effort also received substantial support from other sources. Conclusions regarding the overall project are given in Section 8.

4. Experimental resources

4.1 Experimental equipment: Four categories of experimental equipment were acquired and used:

- (1) A small amount of equipment was acquired to continue already established optical fiber work. A modulator, erbium doped fiber, a MOPA laser diode for pumping the erbium doped fiber, and a diode controller for driving the MOPA laser diode was acquired. Some additional components for the modelocked fiber laser were also acquired as well as incidental equipment for splicing fiber and positioning and aligning fiber elements. Several student senior theses were carried out and students learned how to assemble and operate optical fiber related systems.
- (2) Solid state modelocked laser oscillator and amplifier equipment was acquired for performing spectrally broad measurements with femtosecond time resolution. This equipment was used to develop a source of optical pulses of 100 femtosecond duration, amplify those pulses to energies of several microjoules, generate white light continuum pulses by focusing in a sapphire disk for measurement of photonic band elements, and provide a diagnostic capability in the form a frequency resolved gating experiment using upconversion. A CCD array detector based spectrometer was included, as was a real time autocorrelator. The experimental equipment consisted of a Coherent Innova argon laser, a modelocked Ti:sapphire Mira 900 laser, a RegA 9000 regenerative amplifier, related optical hardware, and Dell computers for processing the experimental data.
- (3) A third set of equipment was acquired in the form of computers for performing calculations and simulations relevant to the photonic band edge structure work. An Intergraph TD-425 was acquired.
- (4) A fourth category of equipment was purchased and used in support of the SEDSAT satellite effort. A satellite Students for the Exploration and Development of Space Satellite number One (SEDSAT-1 or just SEDSAT) was completed and launched on 24-Oct-98. The satellite achieved nominal orbit and activated its transponders after Delta II separation. Telemetry has indicated the internal systems are normal. However, SEDSAT has not responded to subsequent uplink commands. Telemetry has continued to be received allowing evaluation of bus performance and attempts at anomaly resolution. Attempts at anomaly resolution were continued until the end of the SEDSAT portion of this contract, but were not successful.

4.2 Experimental set up:

There were four categories of experimental set-ups. The optical fiber based modelocked oscillator, the white continuum femtosecond metrology system, the computational capability, and the satellite. We detail these below.

4.2.1 Optical fiber based laser oscillator: A harmonically modelocked laser oscillator had been constructed under prior support by AFOSR. Under this support the modelocked laser development was continued with the addition of a second MOPA master oscillator power amplifier and an addition of capability for working with polarization maintaining fiber. Several student projects were carried out using this equipment. The projects addressed various aspects of modelocked laser oscillators including improved stability of the oscillator. An operating laboratory was maintained for the grant period. A capability for training students in fiber optic splicing and related capabilities was retained throughout the effort and continues.

4.2.2 White light femtosecond metrology system: A key experimental set-up was that for white continuum femtosecond metrology. This system included an argon laser, a modelocked Ti:sapphire laser, a regenerative amplifier and associated hardware and stepper motors for performing white light continuum spectroscopy with femtosecond resolution. This system provided a state of the art capability for measuring the transmission and group delay of optical signals transmitted through various photonic structures. In the work under this grant the structures measured were largely photonic band group delay devices fabricated for this effort by personnel at Wright-Patterson AFB. This equipment was purchased in part with AFOSR support and in part with NSF support.

4.2.3 Computer Resources: A TD-425 Intergraph computer was added and used for simulation. Three Jazz drives were added for storing and transporting the simulations of the photonic band structures. Several Dell computers were added for data processing, and monitoring of experiment related information.

4.2.4 Satellite equipment: Components and tools were acquired and used to construct a micro-satellite. More detail is provided in the section below on the satellite portion of this effort.

5. Simultaneous measurement of group delay and transmission of a one-dimensional photonic crystal (Work described in Section 5 was partially supported by this AFOSR contract and in part by NSF and NASA)

The spectrally dependent group delay and the transmission of a layered semiconductor structure were simultaneously measured and exhibited in a single easily interpreted plot. The data spanned a 50 nm wide spectral range with nanometer wavelength resolution, and a 1.3 picosecond wide temporal range with time resolution of a few femtoseconds. Specific data for a 28 period GaAs/AlAs layered photonic band-gap structure that characterizes both group delay and transmission of multiple photonic resonances in a single figure were obtained and compared to theory. This is the first example, to our knowledge, of the simultaneous measurement of both transmission and group delay in a single measurement sequence.

5.1 Introduction to experimental measurement section

Recent experimental and theoretical work has suggested that one-dimensional photonic crystals fabricated from layered semiconductors are an attractive candidate for constructing an optical delay line (ODL) for use in agile beam steering or optical phased arrays [1-3]. It has been shown that for a one-dimensional, N-period, photonic crystal there exists a series of N transmission resonances, a unique feature of which is a combination of large group index with peak transmittance near unity with the largest values occurring in the band-edge resonance [3]. By controlling the frequency location of the transmission resonances, one can, in principle, control and correct spectrally dependent distortions to the group velocity and the phase of the optical pulse. It is consequently important to be able to find means of adjustably controlling the spectral and temporal behavior of these photonic crystals and to evaluate those means of adjustment and control.

Several groups have examined the propagation of ultrashort optical pulses in photonic crystals both experimentally and theoretically [1, 3-5]. The previous experimental work done by Vlasov *et al.* [4] consisted of measuring via auto-correlation methods the delay imparted by a three-dimensional synthetic opal photonic crystal as a function of wavelength. Scalora *et al.* [1] used cross correlation techniques to examine the propagation of a picosecond pulse centered at one particular wavelength transmitted through a one-dimensional layered semiconductor sample as a function of tilt of the sample. Wang *et al.* [5] used autocorrelation methods to measure group delay in a fiber Bragg grating. In all previous work, however, a separate experimental measurement was required to obtain the transmission spectrum of the sample, and separate cycle of delay scan was required for each spectral (or tilt) location. An ideal experiment is one that provides the sample-induced delay of the optical pulse concomitantly with the pulse transmission through the sample in one measurement. The work reported here obtained group delay and transmission measurements by just such a method.

5.2. Theory of Photonic Band-Gap Optical Properties

5.2.1 Group velocity in photonic band-gap structures

To calculate the theoretical group delay caused by a layered semiconductor photonic crystal, the propagation matrix method can be used to first calculate the complex transmission, $t(\omega)$, [1]. The transmission can be expressed as $|t(\omega)|e^{i\phi(\omega)}$, so that the effective group velocity for the structure, $v_g = d\omega/dk = d_{\text{sample}}(d\phi/d\omega)^{-1}$, where d_{sample} is the physical thickness of the sample. For an optical pulse passing through the device, the change in optical path length relative to free space results in a time delay of

$$\text{Delay} = \frac{d_{\text{sample}}}{v_g} - \frac{d_{\text{sample}}}{c} = \frac{d\phi}{d\omega} - \frac{d_{\text{sample}}}{c} \quad 5.2.1$$

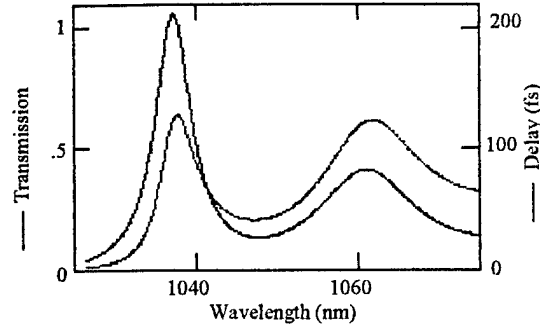


Fig. 5.1. Spectral variation of the theoretical transmission and delay of a 28 period GaAs/AlAs PBG structure.

5.2.2 Measurement technique

To measure the group delay and the transmission shown in Fig. 5.1 in one measurement sequence, a form of SHG-FROG [6] was employed as described by Foing *et al.* [7], using spectrally resolved upconversion of a probe pulse with a reference pulse that has a very narrow spectral width to measure this delay. The upconverted signal produced by mixing two non-collinear plane waves in a non-linear crystal can be expressed by the function [7]:

$$E_{\text{signal}}(\omega, \tau) = f_{\text{Xtal}}(\omega) \int_{-\infty}^{\infty} E_{\text{probe}}(\omega_1) e^{-i\omega_1 \tau} E_{\text{ref}}(\omega - \omega_1) d\omega_1 \quad 5.2.2$$

Where E_{ref} is the reference field, E_{probe} is the probe field, τ is the relative time delay between the reference and the probe, and $f_{\text{Xtal}}(\omega)$ is a function describing the phase matching conditions in the crystal. This function depends on the thickness of the crystal, the angle between the two beams, the angle of the crystal axis, and the frequencies of the two beams.

The spectrum of the reference pulse was approximated as Gaussian, centered on the frequency ω_r , with a small width, $\Delta\omega_r$. Letting $\omega_p = \omega - \omega_r$ and assuming that $\Delta\omega_r$ is small, one can evaluate the magnitude of the probe field at ω_p and keep only the first term in the Taylor series expansion of the phase about ω_p , such that

$$E_p(\omega_1) \approx |E_p(\omega_p)| e^{i[\phi_p(\omega_p) + (\omega_1 - \omega_p)\phi'_p(\omega_p)]} \quad 5.2.3$$

where ϕ' is the first derivative of the phase with respect to ω . It can be further shown that for a given ω_p , the τ dependence of the measured intensity is:

$$I_{\text{signal}}(\omega_p, \tau) = |E_{\text{signal}}(\omega_p, \tau)|^2 \propto e^{-\frac{[\tau - \phi'_p(\omega_p)]^2}{2\Delta\omega_p^{-2}}} \quad 5.2.4$$

which can be seen to be a maximum at $\tau = \phi'_p(\omega_p)$. By curve fitting in time the measured intensity to a Gaussian for each frequency, the location of the peak, $\tau^{\text{max}}(\omega)$, corresponds to the first derivative of the phase of the probe beam. If two measurements are taken, one with the sample in the probe beam, and one without, the delay can be found according to Eq. (5.2.1):

$$\text{Delay}(\omega) = \tau_{\text{Sample}}^{\text{max}}(\omega) - \tau_{\text{NoSample}}^{\text{max}}(\omega) = \phi'_{\text{Sample}}(\omega) - \frac{d_{\text{Sample}}}{c} \quad 5.2.5$$

and the transmission can be obtained as:

$$T(\omega) = \frac{I_{\text{Sample}}[\omega, \tau_{\text{Sample}}^{\text{max}}(\omega)]}{I_{\text{NoSample}}[\omega, \tau_{\text{NoSample}}^{\text{max}}(\omega)]} \quad 5.2.6$$

One should note, here, that the validity of Eq. (5.2.4) depends strongly upon the spectral width of the reference pulse. Also, the above analysis assumes an unchirped reference pulse, or equivalently a pulse sufficiently spectrally narrow \ that any residual chirp is negligible.

5.3 Experiment on Photonic Band-gap Structures

The sample on which the measurements were made was a 28 period GaAs/AlAs one dimensional photonic crystal on a 670 μm GaAs substrate, with the long band edge resonance at 1.038 μm . The structure was fabricated by co-workers of Thomas Nelson at Wright Patterson Air Force Base using molecular beam epitaxy.

The output of a Coherent RegA 9000 regenerative amplifier (the center wavelength is 809 nm, and the spectral bandwidth is ~ 10 nm) was split into a probe and a reference beam. As seen in Fig. 5.2, the probe field was produced by focussing 30% of the laser output into a sapphire flat to generate a continuum, and either allowing the continuum to pass through the sample or not. The reference pulse passes through a prism pair compressor/filter arrangement with a variable slit width included to narrow the reference pulse spectrum. A variable delay stage in the path of the reference pulse allowed control over the relative delay between the probe and reference pulses. The reference and probe pulses were recombined and focussed into a BBO crystal for background free upconversion.

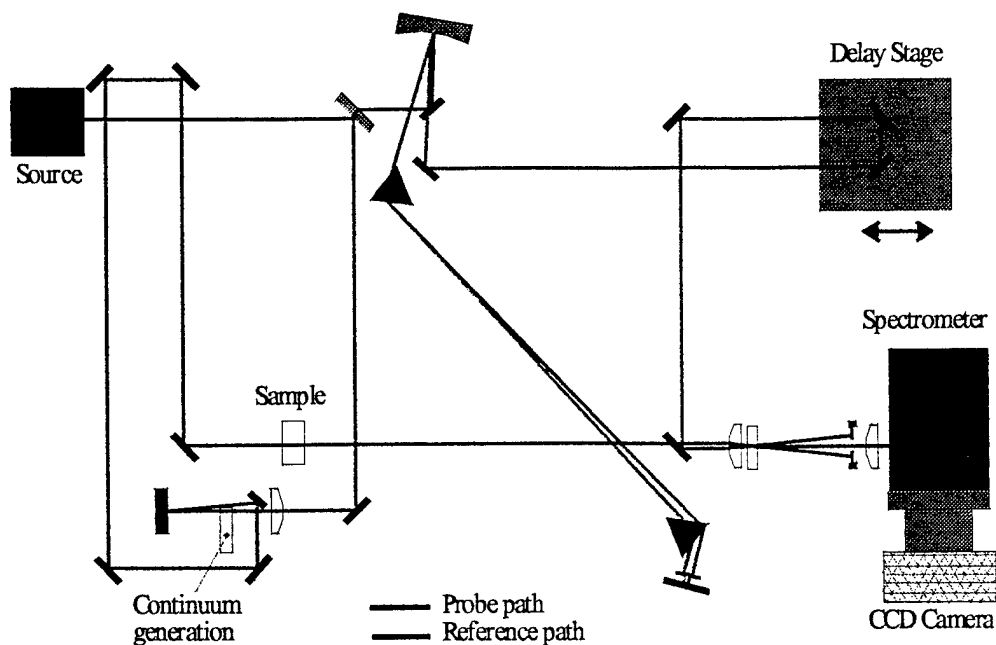


Fig. 5.2. Experimental setup.

Because the probe field was produced by propagating a continuum through the sample, clearly, any variation of group delay or amplitude imparted by the continuum generation process was present in the measured results. Making two sets of measurements, one with the sample in the probe beam path, and one without removed this effect. This makes use of our observation that the continuum is approximately invariant over the time interval between the two measurements. The spectral dependence of the transmission and relative delay imparted by the sample was obtained using equations (5.2.5) and (5.2.6)

For each data set, the variable delay stage was scanned through the region of interest alternately with and without the sample in the probe path until two sets of measurements were made through the sample, and three were made not through the sample. A reference pulse having a spectral width of 1.7 nm was used. All of the like data sets were averaged together, and then for every frequency, were fit to a Gaussian in time to determine the location and magnitude of its maximum. In principle, two scans would suffice, or the use of separated reference and probe paths in a single measurement. We expect to explore these strategies in later work.

5.4. Results of Measurement of Photonic Band-Gap Structure

Figure 5.3 shows the data sets after they were fit to a Gaussian in time for each frequency. The horizontal axis is wavelength and the vertical axis is relative delay. Both data sets span 1332 fs time intervals and 50 nm wavelength intervals.

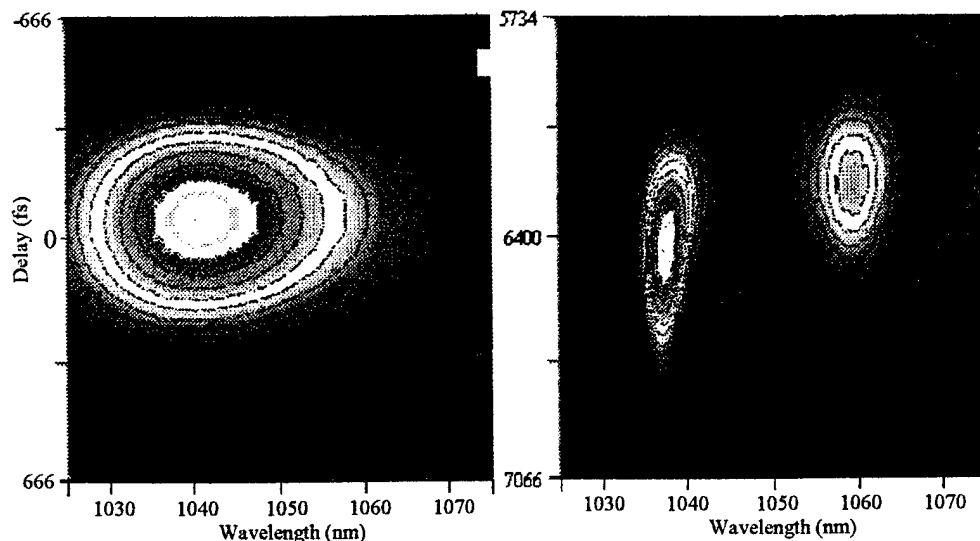


Fig. 5.3. The processed data sets. The leftmost data set represents the upconverted spectral region of the continuum, and the data set on the right is that of the continuum through the sample. For display purposes, here, zero delay has been arbitrarily set to coincide with the center of the continuum data set. The choice of where "zero" is located is not important, as one is interested only in the difference between the delay of the two data sets.

Figures 5.4 and 5.5, respectively, show the transmission and delay recovered from the data shown

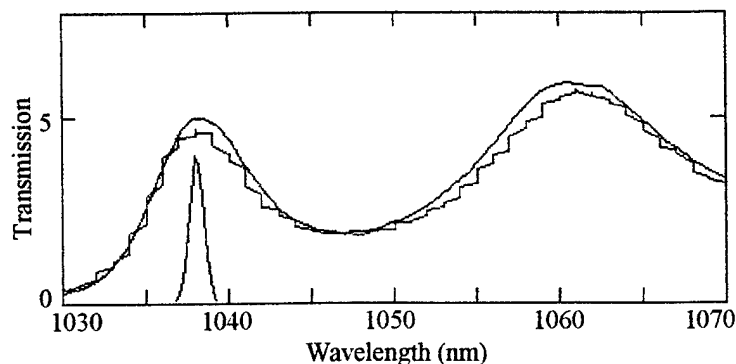


Fig. 5.4. Transmission recovered from data shown in Fig. 5.3 (red) measured at WPAFB (blue). The spectral width of the reference pulse (black), actually centered at 809 nm, is shown here for comparison with the size of the features of the transmission spectrum.

The effect of the group velocity dispersion of the substrate can be clearly seen in the overall slope of the delay in Fig. 5.5. Figure 5.6 shows the delay corrected for this effect by calculating the delay for the substrate and mathematically removing it from both the theoretical and measured results. The measured delay, corrected for the effect of the substrate, can be seen to vary from 200 fs at the peak of the band edge resonance to 27 fs in the first transmission valley.

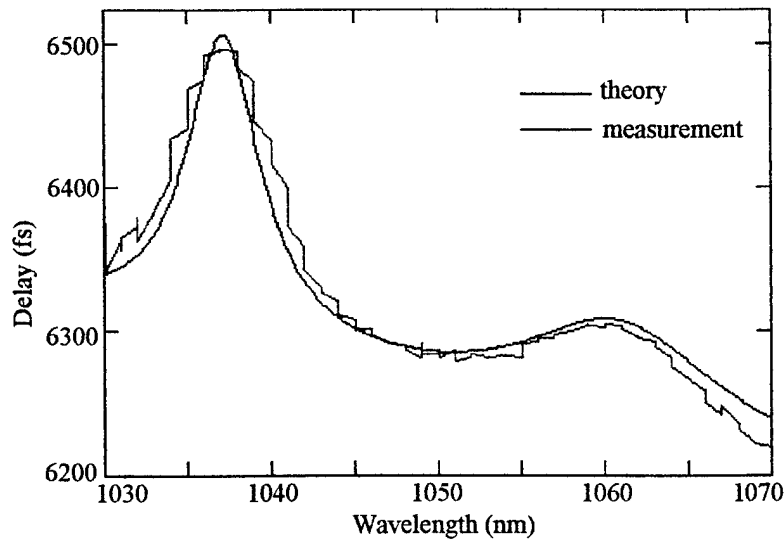


Fig. 5.5. The delay obtained from the data sets shown in Fig. 5.2. The delay imparted by the substrate on which the structure was grown can be seen in the overall downward slope of the delay.

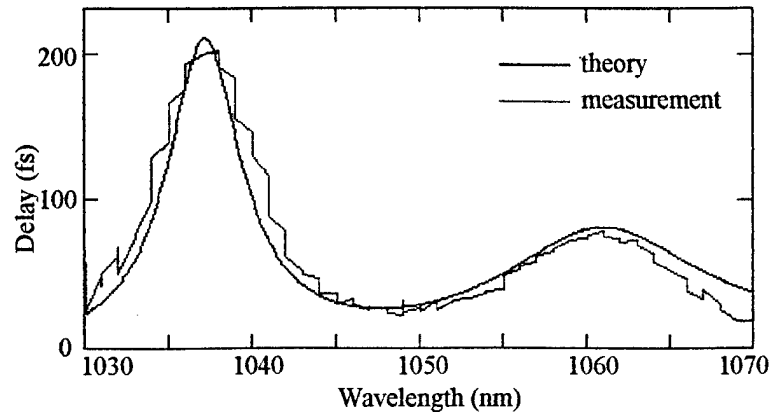


Fig. 5.6. The theoretical and measured delay corrected for the effect of the substrate.

5.5. Conclusions regarding simultaneous measurement of group delay and transmission

The effort demonstrated a measurement technique that provides an easily understood display of the influence of a structure having complex optical properties on a short optical pulse. This technique was applied to the simultaneous measurement of the group delay and spectrally dependent transmission of a one-dimensional photonic crystal. Strong agreement was found between theory and experiment over spectral and temporal ranges that span the pulse duration and multiple photonic resonances. This method should be valuable in studying the spectral and temporal influence of complex optical structures on optical pulses.

6. Colliding pulse element simulation *(A significant part of the support for this portion of the effort was provided by NASA.)*

Calculation and simulation were used to design and characterize a one-dimensional photonic bandedge control and switching element. The goal was means for producing a large adjustable group delay for a short optical pulse in a compact thin film structure. The strategy involves confining a pair of counterpropagating optical pulse in a small resonator, controlling the properties of those pulses, including the relative optical phase, and then switching out a resultant pulse at a particular time. The use of the counterpropagating pair of pulses provides a more stable system that is more easily maintained and adjusted than a single pulse. Group delays amounting to a meter and more of optical path can be achieved in a structure having dimensions of less than a millimeter. To the best of our knowledge means of producing such large delays have not been identified in such small structures by alternative strategies.

In particular, the structure was designed to control and maintain the optical phase relationship of two counterpropagating optical pulses, and hence the resultant pulse formed from the two counterpropagating pulses. The rules for achieving phase coherent switching action, adjustable phase delay, and large

adjustable group delay of the optical pulses were articulated. Applications of arrays of these elements to rapid optical sensing of the relative position of multiple spatially separated points with precision of a small fraction of an optical wavelength was also briefly addressed. The use of two pulses as the form of the signal during the delay process provides a more stable configuration than does a single pulse. The two pulse strategy also lends itself to a dynamic metrology of multiple points in an optical phased array emitter of the type addressed in this study. This latter real time metrology of multiple spatially extended points could prove useful in meeting the demanding requirement of synchronizing multiple spatially extended elements with a precision in time of a small fraction of an optical period.

6.1 Background

Colliding pulse modelocking provided the first reliable access to the femtosecond time domain [8]. The simulation work reported here addressed a colliding pulse structure that differs from the original colliding pulse system in that the pulse "collision" occurs within a fixed, but externally controlled and adjustable, periodic structure. This provided additional capabilities not available in the original colliding pulse system. In that original system the periodic structure that influenced the pulse interaction was entirely induced by the colliding pulses and was not susceptible of external control (aside from the effects of the optical pulses themselves on the medium).

The use of the phase coherent interaction of two short optical pulses with each other in a periodic structure provided an important advance in the control and shaping of optical signals at the time of the discovery of colliding pulse modelocking. In that case the periodically structured optical field produced by the two colliding pulses necessarily exhibited a well defined relationship to the periodic structure of the material system since the optical field induced the periodic structure in the material system as part of the collision process.

For the case of two counterpropagating optical pulses that collide in a fixed periodic structure that pre-exists the collision, the apriori relative phase relationship and physical locations of the two counterpropagating pulses with each other are also important. This requires of the knowledge of, and control of, the relative phase and locations of the optical pulses. A reasonable question concerning these phenomena is whether there are practical applications where such a degree of phase control is both accessible and useful.

The particular case was examined where phase coherent counterpropagating optical pulses are caused to collide periodically within an adjustable one-dimensional photonic band edge element. Design and control of the photonic band edge structure provides means for rapid adjustment of the pulse properties, such as phase and group delay. Means for sensing the relative position of different fixed elements of the surrounding structure were also addressed. The mathematical description of this system was developed and numerical simulations were provided that illustrate this strategy.

One motivation for addressing this technology was the developing need for rapidly adjustable phase coherent optical systems that may span apertures of a meter or more. Under normal conditions the dimensions of these large structures

change by many optical wavelengths in short periods of time. Simply maintaining phase coherence over such an aperture is stressing. The task of sensing these changes accurately, making corrections for those changes, and precisely adjusting the spatial and temporal properties of the optical fields emitted from these large apertures within short periods of time appears difficult without some novel strategy such as identified in the effort reported on here.

6.2 Theory

The periodic structure of interest is a one dimensional photonic bandgap structures (1-D PBG's), composed of parallel, non-absorbing, alternating high and low index of refraction dielectric plates as in quarter wave stacks of reflective coating [1,3]. These structures have traditionally been examined in regard to their role as distributive Bragg reflectors (1-D DBRs) where the periodicity of the lattice prevents excitations within the photonic bandgap from propagating and transmits other excitations (i.e. within the passbands). The attention in this study was directed primarily to the edge of the band gap region where transmission near unity and group delay with control can both be achieved. The recent excellent work by J. Dowling on optical phase in photonic band structures [9], was especially helpful in articulating the detailed phase changes on reflection and transmission from various photonic band edge structures.

Previous work at UAH by the Laser Science and Engineering Group demonstrated that if an optical pulse is incident within the first transmission bandedge resonance of a one dimensional photonic bandgap structure (see Section 5 of this report), an order of magnitude increase in the *group delay* per unit length of an optical element as compared to propagation in free space can be exhibited with nearly invariant transmission [1]. Provided that the spectrum of the pulse is narrow compared with the width of the band edge resonance, Fig. 6.1, minimal distortion occurs

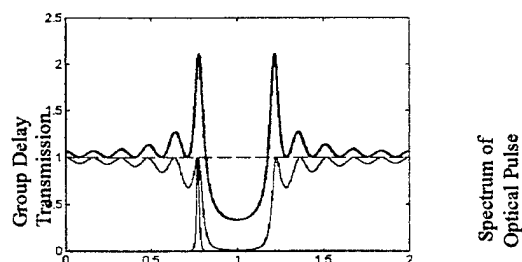


Fig. 6.1. Plot of group delay, pulse spectrum and transmittance

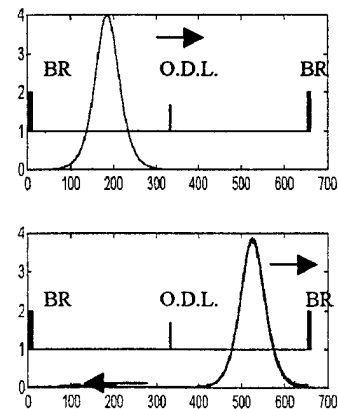


Fig. 6.2 Pulse before and after transmission through photonic optical delay line

Figure 6.2 provides a simulation illustrating this property. The transmitted pulse has a nearly invariant envelope and experiences both *group and phase* delays over which there is some control. Where the center frequency of the incident pulse spectrum coincides with a region of minimum transmittance, the emerging reflected pulse also experiences a large group delay and some nonzero phase delay. This effort focused on a methodology for controlling the *phase delay*, over the full spectral width of both the *transmitted* and *reflected* pulse envelopes, as well as the group delay experienced by those pulses.

6.3 Phase Delay and Phase Dispersion

The frequency and time response of a transmissive resonant one-dimensional photonic band gap structure (i.e., a linear optical element) can be characterized by its complex amplitude reflectivity (or transmittance) spectrum as an optical transfer function:

$$\tilde{H}(\omega) = H(\omega) \exp j \phi(\omega) \quad (6.3.1)$$

Here, $H(\omega)$ represents the *real* amplitude response and $\phi(\omega)$ is the *real* phase response. The tilde (\sim) denotes a phasor. Due to the distributed (multireflection) nature of the quarter wave heterostructure, the stack exhibits a complicated phase and amplitude spectrum (Fig. 6.3).

At the center frequency (i.e., the antiresonance region), the round-trip phase within each structural layer equals an odd multiple of π . For lossless transmissive resonance stacks, the maximum value of the reflectivity occurs at the center of the band gap region where the (real) phase response of the structure is either zero or π , depending on the order of the high and low index values

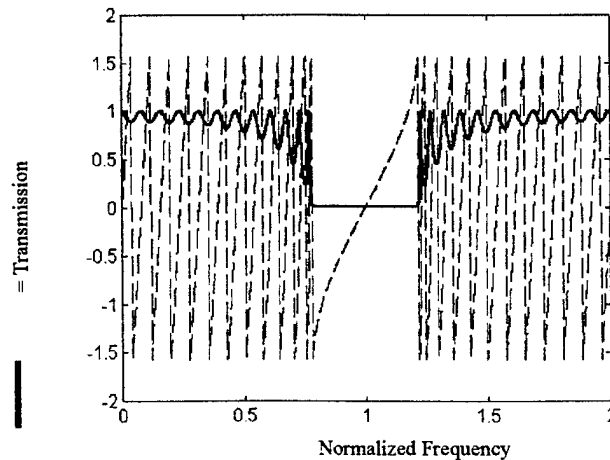


Fig. 6.3. Transmittance spectrum and phase of a 12 period structure where the index of refraction ratio is 1.6667. Dashed line represents the phase (modulo pi) and the solid line represents the spectrum.

The incident field spectrum is related to the field at the output of a multilayered dielectric system as

$$\tilde{E}(\omega) = H(\omega) \exp j \phi(\omega) \tilde{E}_{incident}(\omega) \quad (6.3.2)$$

Here the phase is interpreted as the *phase delay* which a spectral component of frequency ω experiences. Different spectral components of the pulse accumulate different phases as they propagate through the system.

6.4 Accumulation of large net group delay using a single delay element within a resonant structure

This effort sought means of accumulating very large net group delays per unit length of device structure with minimal loss and minimal distortion. One strategy investigated was that of directing an optical pulse within the maximum transmission bandedge resonance peak of an optical delay line positioned precisely at the center of a microresonator. A “left to right” (LTR) going pulse was launched through the delay line and reflected back into the cavity by highly reflective distributed Bragg reflectors for a predetermined number of multiple transits. Simulation results showed that even with nearly invariant transmission, a small amount of “right to left” (RTL) going (or backward traveling) energy propagates toward the left Bragg mirror, strikes the left mirror and is redirected back toward the delay line. As the transmitted and reflected energies couple in the symmetrically positioned delay line, constructive and destructive interference occurs between the redirected pulses within the structure. The simulations showed that without proper phase control of the redistributed energy pulses, multiple passes eventually lead to pulse degradation.

This effort consequently examined a strategy for acquiring multiple passes within the microresonator device structure by dividing the incoming photonic signal into two nearly equal amplitude pulses. A key goal was that of maintaining stable pulses under many transits through the optical delay line. A “fixed, real and linear” dielectric structure was centered in the microresonator and the pulse spectrum centered near a local minimum point of the transmission spectrum. For these conditions the delay line divides the optical pulse into a pair of nearly equal amplitude counterpropagating pulses. The susceptibility of the structure is defined to be purely real (i.e., no absorption or gain) and linear so that quantities such as pulse energy along the length of the structure are conserved. This “two pulse” condition is advantageous in that it enhances sensitivity and maintains the pulse properties over many oscillations in the microresonator with significantly greater stability than for the case of a single pulse. As indicated in Figure 6.4, a local minimum of the transmission spectrum falls near a local minimum of the reciprocal group velocity. In the example a 230 femtosecond duration pulse is directed to strike the structure. The pulse is divided into a pair of counterpropagating photonic pulses.

6.5 Colliding Pulse Switch with Fixed Real Linear Periodic Structures

A device was identified that can perform switching operations on two counterpropagating pulses, referred to here as the propagating left to right (LTR) pulse and the propagating right to left (RTL) pulse. An algorithm was developed that constructs a set of conditions such that the two counterpropagating pulses collide within a fixed dielectric grating and emerge as a single pulse, (i.e., a “colliding pulse switch”, or CPS).

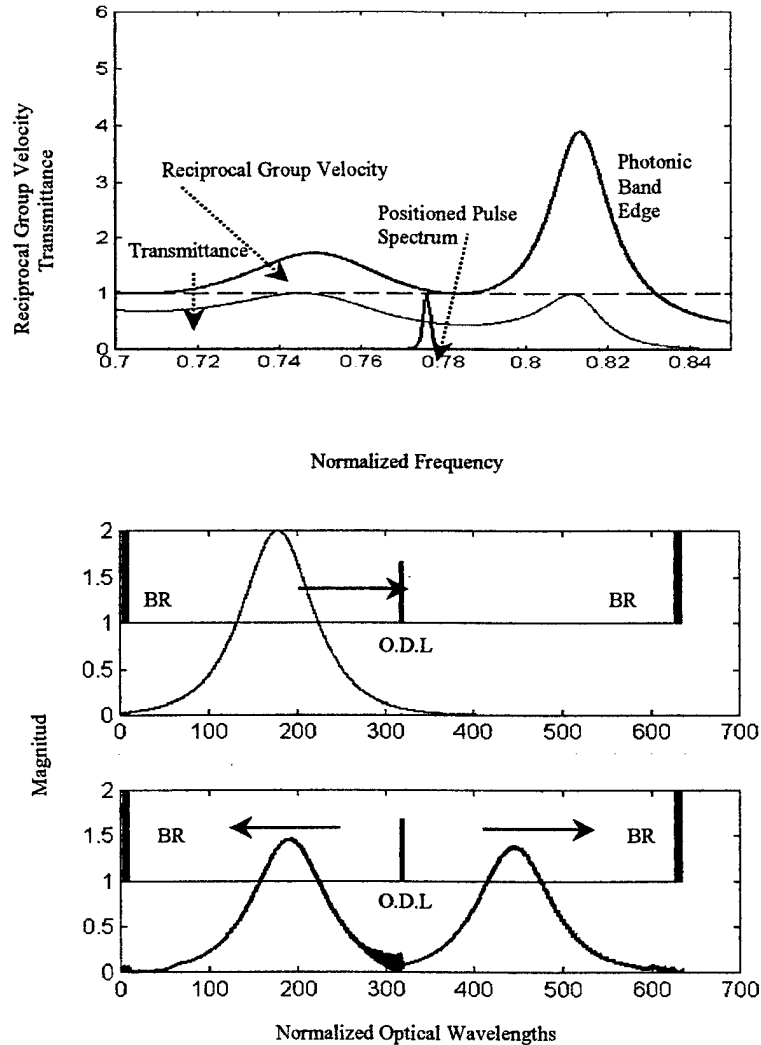


Fig. 6.4. a) Reciprocal group velocity and transmittance spectrum of a 10 period optical delay line ($n_{1,2} = 1.6667$, and 1 respectively). Spectrum of pulse positioned near the inflection point of the band edge resonance.

b) Optical pulse incident on a 10 period optical delay line in a microresonator cavity. Pulse divides into nearly two equal subsignals. (BR = Bragg reflector and O.D.L. = optical delay line)

Particular sets of conditions are specified that result in one of four recombination processes: (1) Two pulses virtually identical to the original two pulses emerge with minimal loss; (2) The two pulses combine into a single pulse directed in the LTR direction with a very small residual energy in the RTL direction; (3) The two pulses combine into a single pulse directed in the RTL direction with a very small residual energy in the LTR direction; (4) Two pulses emerge with different energies that are determined by the relative initial phase of the two pulses. The particular result depends on the phase and amplitude relationships of each pulse relative to the fixed real susceptibility and the phase of the other pulse.

The reconstructed single optical pulse can be emitted from the device by altering the reflective state of one of the Bragg mirrors to a transmissive state. Entrance and exit strategies were identified that achieve that task. Further work will be required to identify means of keeping undesirable distorting mechanisms, such as group velocity dispersion, sufficiently small.

6.5.1 Two Counterpropagating Pulses Directed Toward a Multilayered Stack

The peak of a "right to left" going pulse spectrum can also be matched with the local minimum of the "short wavelength" band edge transmission resonance to divide a pulse into a pair of equal amplitude pulses. By centering a quarter-wave stack in a microresonator cavity with highly reflective Bragg mirrors, one can then establish two counterpropagating pulses. If each counterpropagating pulse is independently launched toward the transmissive resonant structure, "four" pulse components emerge

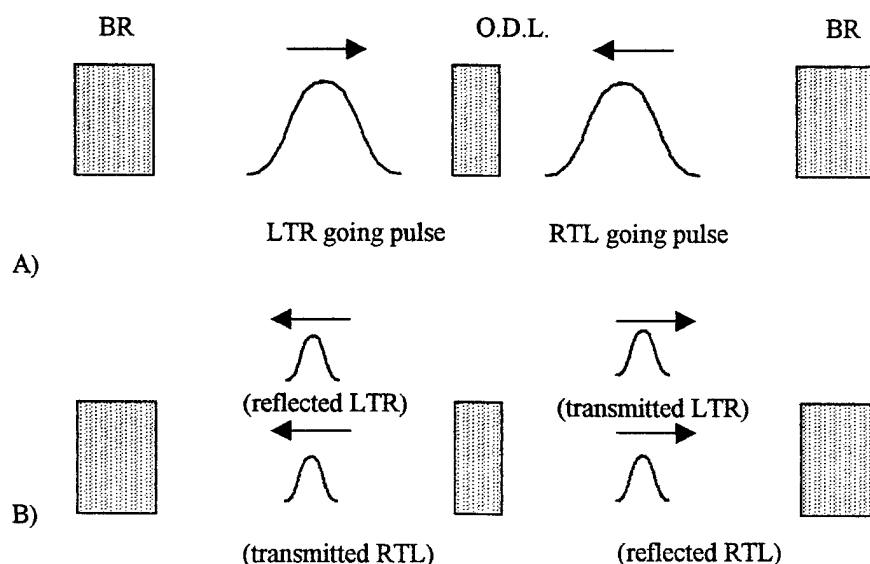


Fig. 5. A) Illustration of colliding pulses in a transmissive resonant structure (i.e. fixed susceptibility). Spectrum of pulse is positioned at the local minimum of the band edge resonance. LTR and RTL optical pulses incident on an N period transmissive resonant structure in a microresonator cavity
B) Pulses divide into four equal subpulses. The four pulses are identified as the reflected LTR, transmitted LTR, reflected RTL and transmitted RTL pulses.

In Figure 6.5 the pulses are identified as the reflected LTR, transmitted LTR, reflected RTL and transmitted RTL pulses. The phase delay each pulse experiences is defined as ϕ_{LTR}^{refl} , ϕ_{LTR}^{trans} , ϕ_{RTL}^{refl} , ϕ_{RTL}^{trans} respectively. The important parameters are those characterizing the phase relationships of the “pairs of pulses” that emerge on either side of the photonic structure. Here, the constructive and destructive processes are similar to those that occur for pulse pairs exiting a Mach-Zehnder interferometer. If the differential phase shift between two pulse components is zero (or an even multiple of π radians), the transmission factor for the resulting pulse is maximized. If the differential phase shift is an odd multiple of π radians, the transmission factor is minimized. In other words, to recombine the emerging pulse on the right side of the structure,

$$\phi_{LTR}^{refl} - \phi_{RTL}^{trans} = \pi \quad (6.5.1)$$

$$\phi_{LTR}^{trans} - \phi_{RTL}^{refl} = 0.$$

To explicate an algorithm for the interference process, ψ_{LTR} was defined as the “initial” phase of the control (or LTR propagating) pulse, and ψ_{RTL} as the “initial” phase of the signal (or RTL going) pulse. The following parameters were also defined:

$$\Delta \phi_{LTR}^{refl} = \phi_{LTR}^{refl} - \psi_{LTR} \quad (6.5.2)$$

as the difference in phase a LTR pulse experiences upon reflection,

$$\Delta \phi_{LTR}^{trans} = \phi_{LTR}^{trans} - \psi_{RTL} \quad (6.5.3)$$

as the difference in phase for a LTR going pulse experiences upon transmission,

$$\Delta \phi_{RTL}^{refl} = \phi_{RTL}^{refl} - \psi_{RTL} \quad (6.5.4)$$

as the difference in phase a RTL pulse experiences upon reflection, and

$$\Delta \phi_{RTL}^{trans} = \phi_{RTL}^{trans} - \psi_{LTR} \quad (6.5.5)$$

as the difference in phase a RTL pulse experiences upon transmission.

Equation 6.5.1 can be re-written in terms of Equations 6.5.2 – 6.5.5. The result is

$$(\psi_{LTR} - \psi_{RTL}) + (\Delta \phi_{LTR}^{trans} + \Delta \phi_{RTL}^{refl}) = 0 \quad (6.5.6)$$

Using a similar strategy, an expression was derived for a pulse emerging on the right side of the structure as

$$(\psi_{LTR} - \psi_{RTL}) + (\Delta \phi_{LTR}^{trans} + \Delta \phi_{RTL}^{refl}) = \pi \quad (6.5.7)$$

These equations express the phase conditions necessary to recombine two counterpropagating “nearly equal amplitude” pulses that are simultaneously and symmetrically launched to strike a quarter-wave stack.

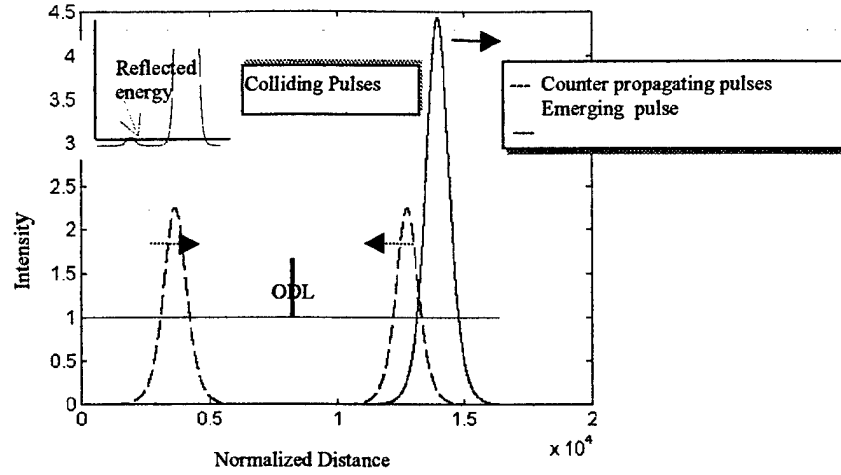


Fig. 6.6 A pair of pulses collide in a fixed real linear transmissive resonant structure and emerge as a single optical pulse

One way of characterizing the rules given above is to view them as *keeping track of* the changes in phase that the pulses experience after they strike each dielectric periodic structure in the device design. For pulses that strike and reflect from the Bragg mirrors, a similar ‘bookkeeping process’ was required to account for penetration delay (i.e. the effective depth inside the mirror at which the optical pulse reflected).

The case was examined where two equal amplitude subpulses are simultaneously redirected by the left and right Bragg reflectors in a microresonator Fig. 6.6. The initial conditions for the two pulses were written as

$$\begin{aligned} A_{initial\ 1} &= Amplitude_1 \times \frac{1}{\cosh(2 \times Z_0 [z - loc_1])} \\ A_{initial\ 2} &= Amplitude_2 \times \frac{1}{\cosh(2 \times Z_0 [z - loc_2])} \left[\exp\left(-i2zn\left(\frac{2\pi}{q}\right)\right) \right], \end{aligned} \quad (6.5.8)$$

where $(z - loc_1)$ defines where the pulse was located in the “real” space window, Z_0 defines the pulse width, and the amplitude was determined by the *amplitude* coefficient. The exponential term in A_{init2} , $\left[\exp\left(-i2zn\left(\frac{2\pi}{q}\right)\right) \right]$, propagated the

pulse in the “right to left” direction. The initial phase of the pulse evolution was set to zero and the appropriate wavelength (q value) was selected.

In this simulation the control pulse (on the left side of structure propagating toward the right of the real space window) and the signal pulse (on right side of structure propagating toward the left of the real space window) are at the same distance from the center of the structure. Varying the phase of the “left to right” going pulse by a predetermined value before launching both pulses toward the structure illustrates how the resultant behavior is controlled.

The conditions were then chosen to satisfy the conditions for Equation 6.5.6 for ψ_{LTR} and to consequently demonstrate how the pulses recombine on the right side of the structure if the phase profile of the “left to right” going pulse is altered by the correct value. The result of the simulation is illustrated in Figure 6.6. For the recombined pulse to emerge on the left side of the structure, the conditions in Equation 6.5.7 must conversely be satisfied.

Work was done to evaluate the phase of LTR and RTL reflected and transmitted pulses under general conditions. In particular, if the stack in the middle of the resonator is symmetric as opposed to asymmetric, the transmitted and reflected subpulses emerge from the structure simultaneously. This simplifies the task of designing the constructive and destructive interaction process in that the symmetric index potential imparts the same time delay and phase to both transmitted and reflected pulses with no relative phase difference or time delay difference.

This part of the effort described a “colliding pulse switch” that depends only on the *phase relationship* of two counterpropagating pulses. There exists a set of conditions between the relative phase profiles across two counterpropagating equal amplitude pulses, where the signal and control pulse will recombine and emerge with a nearly invariant intensity profile.

6.6. Absolute Change in Phase Upon Reflection and Transmission for Symmetric and Asymmetric Structures

6.6.1 Absolute Change in Phase Upon Transmission

Effort was directed toward specifying clearly the *change in phase* experienced by an optical pulse that has been transmitted through a linear optical element. The case was examined (for a single layer structure) of a pulse of light incident from the left. The phase of the emerging light pulse can be thought of as the aggregate phase accumulated by a plane wave as it traverses the structure. If the structure’s total thickness is a length d , the phase thickness of the structure is equivalent to the product of the effective wavenumber and the structure thickness, $\phi = k_{eff} d$.

As a pulse traverses a quarter wave structure, it experiences a phase delay (i.e., change in phase) *relative* to the same pulse if that pulse propagated through free space. The *absolute change in phase upon transmission* is defined here as the difference in phase for the signal that has been *transmitted* through a high index layer (or post) as compared to the phase that would have been accumulated if the pulse had propagated through free space. This change in phase is

$$\Delta \phi = \frac{2\pi (n_s - n_o) d}{\lambda}. \quad (6.6.1)$$

In the simulation model, “d” defined the length of the structure (in grid points), λ represented the number of grid points that defined an optical wavelength, n_o was the background index (i.e., unity since it was assumed that the pulse was propagating in free space) and n_s was the index of refraction for the high index layer. This information is sufficient to predict the phase change, in radians, for a pulse that has been *transmitted* through a unit cell.

6.6.2 Absolute Change in Phase Upon Reflection

The absolute *change in phase upon reflection* for an optical pulse incident upon a high index post was also examined. For the simplest case (i.e. a single layer between two semi-infinite regions), the well known Fresnel formula defines the reflection coefficient as

$$r = \frac{r_1 + r_2 \exp(-i2\delta)}{1 + r_1 r_2 \exp(-i2\delta)}, \quad (6.6.2)$$

where δ is the phase thickness of the layer (i.e., $\delta = \frac{2\pi}{\lambda} nd$), r_i is the amplitude reflectance of the i^{th} interface as given above, λ is the wavelength and the product “(nd)” is the optical thickness of the layer (see any standard optic text).

To assign the phase factor, a hypothetical pulse propagating in free space was used as the reference. The *change in reflection phase* at the incident interface is defined as the phase of the pulse that reflects off the interface (i.e., π) minus the additional phase accumulated by the part of the pulse that propagates a distance equivalent to the distance to the midpoint of the structure and back to the air / post interface.

$$\begin{aligned} \phi_{\text{reflected}}^{\text{Left to right}} &= \pi - \left[2 \left(\frac{d}{2} \right) \left(\frac{2\pi}{\lambda} \right) \right] \\ &= \pi \left(1 - \frac{2d}{\lambda} \right) \end{aligned} \quad (6.6.3)$$

This approach amounts to defining a particular “clock” pulse as the reference pulse for the system. The clock pulse propagates in free space in the (LTR) direction. In contrast, a reflected pulse was described as a pulse launched in the same direction as the reference pulse, but as reflecting at the *middle* of the high index layer and then propagating back in the direction opposite to the initial direction [9].

Conflicting results were encountered in the simulations when pulses were reflected off of quarter wave posts described by an odd number of grid points versus quarter wave posts described by an even number of grid points (Equation 6.6.4).

$$\begin{aligned}\phi_{\text{reflected}}^{\text{Right to left}} &= \pi - \left[2 \left(\frac{d}{2} \right) \left(\frac{2\pi}{\lambda} \right) \right] \pm \phi_{\text{extra phase term}} \\ &= \pi \left(1 - \frac{2d}{\lambda} \right) \pm \phi_{\text{extra phase term}}.\end{aligned}\tag{6.6.4}$$

Dowling was investigating an analytic calculation to explain the symmetry relations between phases of transmitted and reflected pulses from one dimensional quarter wave stacks at the same time this study was investigating this problem [9].

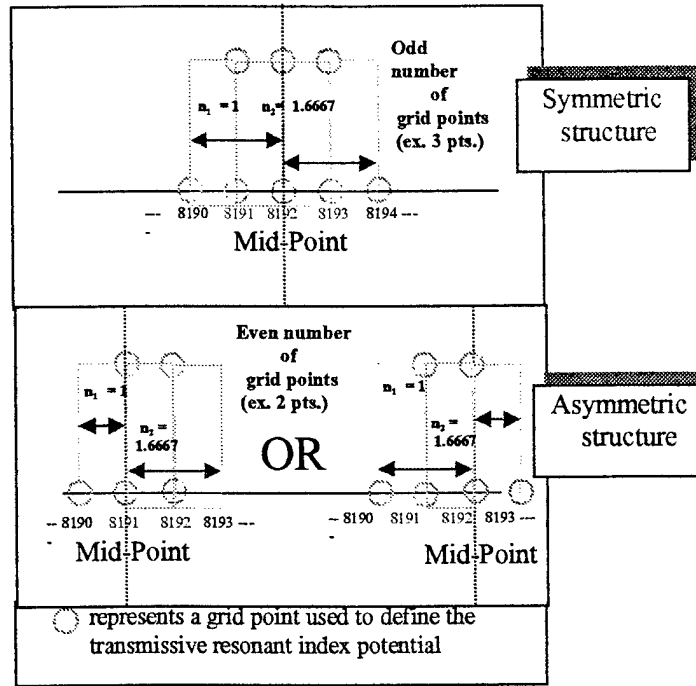


Fig. 6.7. Example of how the code distinguishes a symmetric index potential from an asymmetric transmissive resonant index potential. A post defined by an odd number of grid points is characterized as a symmetric post. An index potential characterized by an even number of grid points is asymmetric in that there is not a well defined mid-point (or center grid point) in the structure.

Dowling demonstrated that as a direct consequence of energy conservation, parity conservation and time reversal symmetry, transmission amplitude, transmission phase and reflection amplitude are equivalent for RTL and LTR processes. Dowling showed the reflection phases of the RTL versus LTR process are not equivalent, as described by

$$\phi_{RTL}^{ref} = 2\phi_{LTR}^{trans} - \phi_{LTR}^{ref} \pm \pi \pm 2\pi m, \quad (6.6.5)$$

and that this is a direct consequence of the symmetry of the unit cell. A LTR traveling pulse must traverse an extra quarter wave distance before it strikes the high index post as compared to the RTL pulse which strikes the high index immediately and reflects before it reaches the mid point of the unit cell [9].

An examination of the simulated structures revealed that posts characterized by an even number of grid points are, in effect, asymmetric. This occurs because the mid – point is not well-defined by the code. An index potential constructed from an odd number of points has a well-defined center point and is categorized as spatially symmetric. In the special case where the index structure is spatially symmetric (e.g., semi-reflecting symmetric lossless mirrors), it is well documented that the phase shift difference between transmitting and reflecting

wave fields equals $\frac{\pi}{2}$. Therefore, when a quarter-wave post is described with an odd number of grid points, this also defines the symmetry of the post and consequentially the phase relationship between reflected and transmitted fields.

To differentiate physical phase variations from nonphysical contributions from the simulation algorithms, care was taken to correctly interpret the control over the phase (i.e. phase delay) experienced by an optical pulse that is incident, reflected and transmitted from a transmissive resonant structure.

A methodology was developed in this effort showing how to use a predetermined “change in phase” to predict constructive and destructive interference within quarter wave periodic media. An algorithm was developed to construct a “phase only dependent” pulse switch when two equal amplitude counterpropagating pulses “collide” at the local minimum of the transmission bandedge resonance of a quarterwave stack.

6.7 Numerical model

6.7.1 Pulse propagation in one dimensional photonic bandgap dielectric structures

The dynamics of a pulse striking, transmitting through, and reflecting from a multilayered stack were modeled by using a “modified version” of the well known beam propagation method (FFT-BPM) [10]. This modified version is advantageous in that it can “handle reflections” without explicitly detailing the boundary conditions for the fields at each interface. This is in contrast to the *conventional* beam propagation method that invokes the use of the slowly varying envelope approximation (SVEA). This difference is important in that the SVEA

neglects the counterpropagating field component generated by the polarization vector (i.e., it will not display reflective field components).

Formulas expressing the transmittance function of a finite N period multilayered stack and the reciprocal group velocity of a finite N period multilayered stack were used to numerically step pulses in time through particular spectral regimes of interest. The assumption was made that the optical fields encounter the same position dependent index of refraction regardless of polarization or direction of propagation.

The scalar equation describing the interaction of light with matter for the positive frequency component envelope functions is written as

$$\frac{\partial^2 E}{\partial z^2} - \frac{1}{c^2} \frac{\partial^2 E}{\partial t^2} + 2ik \frac{\partial E}{\partial z} + \frac{2i\omega}{c^2} \frac{\partial E}{\partial t} + \nabla_T^2 E = \frac{4\pi}{c^2} \left(\frac{\partial^2 P}{\partial t^2} - 2i\omega \frac{\partial P}{\partial t} - \omega^2 P \right) \quad (6.7.1)$$

where E and P are the electric field and polarization envelope functions respectively [10]. For convenience, the longitudinal and transverse coordinates are scaled with respect to the input wavelength, and the equation is re-expressed as

$$\left(\frac{i}{4\pi} \frac{\partial^2}{\partial \xi^2} - \frac{i}{4\pi} \frac{\partial^2}{\partial \tau^2} - \frac{\partial}{\partial \xi} + \frac{i}{4\pi} \nabla_{\perp}^2 \right) E - \frac{\partial E}{\partial \xi} = i \left(\frac{\partial^2 P}{\partial \tau^2} + 4\pi \frac{\partial P}{\partial \tau} - 4\pi^2 P \right) \quad (6.7.2)$$

where $\xi = z/\lambda$, $x = x/\lambda$, $y = y/\lambda$ and $\nabla_{\perp}^2 = \lambda^2 \nabla_T^2$. By defining the free space propagator as

$$\hat{D} = \frac{i}{4\pi} \frac{\partial^2}{\partial \xi^2} - \frac{i}{4\pi} \frac{\partial^2}{\partial \tau^2} - \frac{\partial}{\partial \xi} + \frac{i}{4\pi} \nabla_{\perp}^2, \quad (6.7.3)$$

the potential operator as

$$\hat{N}E = -i \left(\frac{\partial^2 P}{\partial \tau^2} - 4\pi i \frac{\partial P}{\partial \tau} - 4\pi^2 P \right), \quad (6.7.4)$$

and omitting the higher order time derivatives, (i.e., the slowly varying envelope with respect to time (SVEAT) holds) [10,14], the equation of motion can be rewritten as

$$\frac{\partial^2 E}{\partial \xi^2} + 4\pi i \frac{\partial E}{\partial \xi} + 4\pi i \frac{\partial E}{\partial \tau} = -4\pi^2 \left[(n^2 - 1) \right] E \quad (6.7.5)$$

where the polarization is given by $P = \chi E = \frac{n^2(\xi) - 1}{4\pi} E$, and time is scaled by the corresponding optical period as

$$\tau = ct/\lambda \quad (6.7.6)$$

for convenience. Solving for the free space propagator separately and taking the Fourier transform of Equation 4.5 with respect to spatial coordinate ξ , results in

$$\tilde{E}(\kappa, \tau + \Delta\tau) = \tilde{E}(\kappa, \tau) e^{-i\pi(\kappa^2 + 2\kappa)\delta\tau} \quad (6.7.7)$$

(where the Fourier integral is computationally solved in the form of a discrete Fourier transform in wave number space for a propagation distance of $\delta\tau$). It is the κ^2 term in the free space propagation operator that accounts for counterpropagating waves.

By neglecting the free space operator, refraction in the medium can be written as

$$E(\xi, \tau + \Delta\tau) = E(\xi, \tau) e^{i\pi(n^2 - 1)\delta\tau} \quad (6.7.8)$$

for a propagation distance of $\delta\tau$. However, one must be careful in how the propagation distance interpretation affects pulse description. The “split-step” beam propagation method is an iterative scheme that advances the field in time by small step sizes, $\delta\tau$. The algorithm was tested by varying the spatial window size (which is related to the frequency window size) and by changing the number of FFT (Fast Fourier Transform) points. Results were compared to the literature on the modified beam propagation method. Independent programs were extensively tested for accuracy and reliability. The numerical value of 0.01 was empirically identified as an acceptable choice for $\delta\tau$. This choice was validated by calculating the pulse energy, a conserved quantity in the absence of absorption and/or gain. The real space window was set to 16384 points and was wide enough to ensure that pulse energy remained confined within the window. Pulse widths ranged between 70 - 100 optical wavelengths, and the spatial windows were ~ 8 -12 times the full width half maximum (FWHM) values of the pulse. As a consequence of the periodic boundary conditions imposed by the FFT transform, numerical instabilities result when the pulse energy is wide enough to hit the edges of the real space window (i.e., are able to *wrap-around* to the other side of the window). Although absorbing boundary conditions [11] are often used to artificially absorb radiation reaching the edges of the window, this condition was not necessary. This multilayered Bragg reflector mirrors positioned at the edges of the windows reflect optical energy back into the window and prohibit wrap around at the edges.

The carrier frequencies of the simulated optical pulses were spectrally positioned to explore the conditions identified above. With $\delta\tau = 0.01$, Equation

7.6 becomes $0.01 = \left(\frac{1}{T}\right) dt$, where T is defined to be one optical period. To

propagate an optical pulse in real space, the split-step method requires a number of iterations (i.e., intersteps) of the forward and inverse Fourier transforms.

Defining the number of intersteps as n_i and N as the number of grid points, a pulse can be displaced by a predetermined number of grid points by the equation $n_i dt = N$. For example, for a fixed value of $dt=0.01$, displacement of a pulse by

one grid point requires 100 intersteps. Since $f = \frac{1}{T} = \frac{c}{\lambda}$, this relation can be re-written in terms of dt , as $\frac{n_i}{N} = \frac{1}{(0.1)T}$.

To investigate the interaction of a pulse with a photonic structure, a grid point resolution better than an optical wavelength was required. In other words, a wavelength was required to be number of grid points large compared to one. This was addressed by writing Equation 6.7.6 as

$$\delta\tau = q \left(\frac{c dt}{\lambda} \right), \quad (6.7.9)$$

where q represents the number of grid points necessary to define one wavelength of an optical pulse. One can also redefine the Fourier transform frequency variable κ_{freq} as

$$\kappa_{freq} = q \left(\frac{c}{\lambda} \right) = q \left(\frac{1}{T} \right) \quad (6.7.10)$$

For this work, the number of grid points used to define one optical wavelength (i.e., q values) was typically between 20 and 30 given the 16,384 points in the computational window. If this condition was not satisfied distortions occurred. We believe that this was primarily a consequence of the $\exp(-i2\pi\kappa\delta\tau)$ factor in the free space operator (Equation 6.7.7). When $\kappa\delta\tau$ is equivalent to unity, the phase factor equals 2π (i.e., a periodic boundary condition is reached) and the pulse reproduces itself. To work well within this condition, the product of the frequency space and normalized propagation distance variables must be small with respect to unity. When q is increased, κ increases and amplitude distortions appear.

Computer programs were entirely written using MATLAB Version 4.2c.1. Codes were chosen and monitored to ensure a high degree of accuracy. The step size was adjusted so that the accumulated phase corrections per step was minimal ($\delta\tau = 0.01$).

To address cases of interest in current literature a relatively large bandwidth for the device was used. Hence a number of periods that was not too large, e.g., $N < 100$ was required. A ratio of high to low index not too close to unity was also imposed (e.g., $n_1 / n_2 \geq 1.25$). Bendickson, et al. noted that altering the layer thickness and/or the number of unit cells in the structure has the consequence of altering the bandwidth of the transmission resonance. This is important in that optimum performance of the device requires proper choice of the bandwidth, needed delay, etc.

Hyperbolic secant optical pulses with pulse durations of ~230 femtoseconds were introduced in the model so as to strike various regions of the transmission bandedge. Structures of 10 periods of alternating index refraction values of 1.6667 and 1 respectively were used for this part of the simulation work. The

index values were chosen to simplify the calculation rather than to typify a particular set of materials.

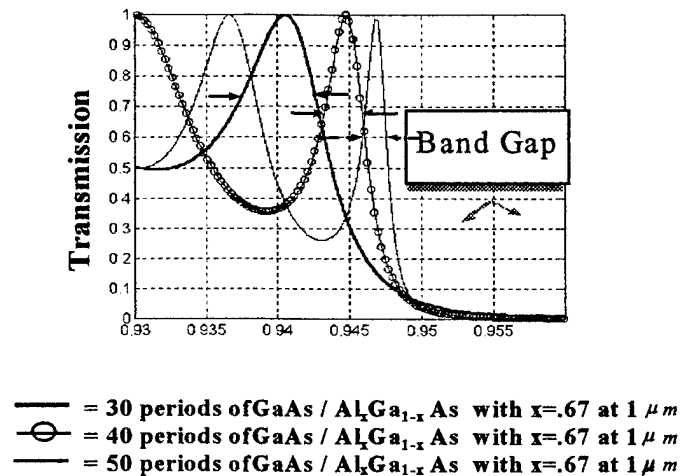


Fig. 6.8 Photonic bandedge of a transmissive resonant structure varies as the number of periods are increased

6.8 Experimental Demonstration of Controlled Photonic Band Elements

Individual photonic structures that illustrate the electronically or optically controlled variation in the bandedge have been built by the group at Wright Lab and examined experimental set-up. The change in index for applied voltage is relatively small. The change in index with optical carrier injection appears sufficiently large to be of interest. Current work addresses this area and we expect it to be more fully addressed under future work [12].

6.9 Summary of Findings

The effort simulated and described one-dimensional photonic structures that provide control of both the phase delay and the group delay of short optical pulses. Structures composed of multiple photonic elements were identified that can, given sufficiently rapid switching and solution of challenging fabrication tasks, provided large adjustable group delay in compact low mass structures suitable for microspacecraft.

Further work will be required to achieve operating systems utilizing the structures identified, demonstrated and evaluated in this effort. Current work under other support is addressing use of free space amplifiers that efficiently convert laser diode pump power into solid state laser emission at high average power. A strategy that bears some analogy to that used in double clad fiber can be used in this free space approach. An advantage is gained in that the beam intensities and total average power can be considerably higher.

7. 0 References

1. M. Scalora, R. J. Flynn, S. B. Reinhardt, R. L. Fork, M. J. Bloemer, M. D. Tocci, C. M. Bowden, H. S. Ledbetter, J. M. Bendickson, R. P. Leavitt, "Ultrashort pulse propagation at the photonic band edge: Large tunable group delay with minimal distortion and loss," *Phys. Rev. E* **54**, R1078-R1081 (1996)
2. T. R. Nelson, J. P. Loehr, Q. Xie, J. E. Ehret, J. E. VanNostrand, L. J. Gamble, D. K. Jones, S. T. Cole, R. A. Trimm, W. M. Diffey, R. L. Fork, A. S. Keys, "Electrically tunable group delays using quantum wells in a distributed Bragg reflector," in *Enabling Photonic Technologies for Aerospace Applications*, Proc. SPIE 3714, 12-23 (1999)
3. J. M. Bendickson, J. P. Dowling, M. Scalora, "Analytic expressions for the electromagnetic mode density in finite, one-dimensional, photonic band-gap structures," *Phys. Rev. E* **53**, 4101-4121 (1996)
4. Y. A. Vlasov, S. Petit, G. Klein, B. Honerlange, C. Hirleimann, "Femtosecond measurements of the time of flight of photons in a three-dimensional photonic crystal," *Phys. Rev. E* **60**, 1030-1035 (1999)
5. S. Wang, H. Erlig, H. R. Fetterman, E. Yablonovitch, V. Grubsky, D. S. Starodubov, J. Feinberg, "Measurement of the temporal delay of a light pulse through a one-dimensional photonic crystal," *Micro. Opt. Technol. Let.* **20**, 17-21 (1999)
6. R. Trebino, K. W. Delong, D. N. Fittinghoff, J. N. Sweetser, D. J. Kane, "Measuring ultrashort laser pulses in the time-frequency domain using frequency-resolved optical gating," *Rev. Sci. Instrum.* **68**, 3277-3295 (1997)
7. J. P. Foing, J. P. Likforman, M. Joffre, A. Migus, "Femtosecond pulse phase measurement by spectrally resolved up-conversion: Application to continuum compression," *IEEE J. Quantum Electron* **28**, 2285-2290 (1992)
8. R. Fork, B. I. Greene and C.V. Shank, "Generation of optical pulses shorter than 0.1 psec. by colliding modelocked lasers," *Appl. Phys. Let.* **38**, 671-672 (1981).
9. J. P. Dowling, "Parity time reversal and group delay for inhomogeneous dielectric slabs: applications to pulse propagation in finite one dimensional, photonic bandgap structures," *IEE Proc. - Optoelectronics*, **145**, 420-435 (1998).
10. M. Scalora and M. Crenshaw, "A beam propagation method that handles reflections," *Optics Comm.* **108**, 191-196 (1994).
11. D. Yevick and Jun Yu, "Optimal absorbing boundary conditions," *J. Opt. Soc. Am. A* **12**, 107-110 (1995).
12. L. J. Gamble, W. M. Diffey, S. T. Cole, R. L. Fork, D. K. Jones, T. R. Nelson Jr., J. P. Loehr, J. E. Ehret, "Simultaneous measurement of group delay and transmission of a one dimensional photonic crystal," *Optics Express* **5**, 267-272 (1990),
<http://www.opticsexpress.org/opticsexpress/topbiframe.htm>.

8.0 Personnel supported or associated with the effort.

Richard L. Fork: Professor of Electrical and Computer Engineering, UAH

John O. Dimmock: Professor of Physics, UAH

Michael Jones: Postdoctoral Student in Electrical and Computer Engineering

Spencer T. Cole: Graduate student in Electrical and Computer Engineering

Andrew S. Keys: Graduate student in Electrical and Computer Engineering

Darryl K. Jones: Graduate Student in Optical Science and Engineering

Lisa J. Gamble: Graduate Student in Optical Science and Engineering

Clifford Pate: Undergraduate student

Kate Horton: Undergraduate student

Rebecca A. Trimm: : Undergraduate student

John Dimmock, Jr.: Undergraduate student

9.0 Publications in Peer-reviewed Journals

1. L. J. Gamble, W. M. Diffey, S. T. Cole, R. L. Fork, D. K. Jones, T. R. Nelson Jr., J. P. Loehr, J. E. Ehret, "Simultaneous measurement of group delay and transmission of a one dimensional photonic crystal," *Optics Express* **5**, 267-272 (1990), <http://www.opticsexpress.org/opticsexpress/topbiframe.htm>.
2. "Optical Amplifier for Space Applications", Richard L. Fork, Spencer T. Cole, Lisa J. Gamble, William M. Diffey, and Andrew S. Keys, *Optics Express* **5**, 292-301 (1999).
3. M. Scalora, R. J. Flynn, S. B. Reinhardt, R. L. Fork, M. J. Bloemer, M. D. Tocci, C. M. Bowden, H. S. Ledbetter, J. M. Bendickson, J. P. Dowling and R. P. Leavitt, "Ultrashort pulse propagation at the photonic band edge: Large tunable group delay with minimal distortion and loss," *Phys. Rev. E* **54**, R1078-R1081 (1996).

10.0 Interactions/Transitions

a. Participation/presentations at meetings, conferences, seminars,

1. "Resonant Transmissive Modulator Construction for Use in Beam Steering Array", Andrew S. Keys, Richard L. Fork, Thomas R. Nelson, Jr., and John P. Loehr, *SPIE Proceedings* **3787** "Optical Scanning and Design Applications" (1999).
2. "Electrically Tunable Group Delays Using Quantum Wells in a Distributed Bragg Reflector", Thomas R. Nelson, Jr., John P. Loehr, Qiang Xie, James

E. Ehret, Joseph E. Van Nostrand, Lisa J. Gamble, Darryl K. Jones, Spencer T. Cole, Rebecca A. Trimm, William M. Diffey, Richard L. Fork, and Andrew S. Keys, SPIE Proceedings 3714, (1998).

3. "Agile Steering of Optical Beams Using Photonic Band Edge Devices", Richard L. Fork and Spencer T. Cole, DARPA/ETO Meeting, Crystal City, VA March 23, 1999.
4. "Spatially Extended Modelocking", Richard L. Fork, Lisa J. Gamble, Brian M. Robinson, and Spencer T. Cole, Laser Physics 99 UNESCO Conference (Invited), Budapest, Hungary July 4, 1999.
5. "Spatially Extended Agile Modelocking", Darryl K. Jones and Richard L. Fork, Paper WLL137, Sept 29, Optical Society of America Santa Clara CA 1999.

Talks at Universities:

"Agilely Controlled Optical Beam Steering" Physics Colloquium at University of Alabama in Birmingham: May 21, 1999

"Novel Optical Gyroscopes", Seminar at University of Alabama, Tuscaloosa, June 1999.

b. Consultative and advisory functions to other laboratories and agencies

- i. Consulting on the Space Based Laser (laser diode component) for BMDO managed by ANSER and USRA.
- ii. Consulting on Advanced Discriminating Laser Technology (for Space and Missile Defense Command through Army Air and Missile Command)
- iii. Consulting on Distributed Space Solar Power (managed by NASA)
- iv. Interaction with Wright Lab on Photonic Band Structures. Data from our measurements were made available to Tom Nelson of Wright Labs. We evaluated photonic band structures fabricated in the Wright Lab facility.

10.0 New discoveries, inventions, or patent disclosures

A patent application was awarded by the United States Patent and Trademark Office. The title is "Microresonator and Associated Method for Producing and Controlling Photonic Signals with a Photonic Bandgap Delay Apparatus". Patent # 6,028,693 Filed 1/14/98. Awarded 2/22/00.

A patent application was awarded by the United States Patent and Trademark Office. The title is "Photonic Bandgap Apparatus and Method for Delaying Photonic Signals". Patent #5,751,466. Issued 05/12/98. (Patent was filed prior to start of work, but effort assisted in obtaining the final patent award.)

12.0 Societal Honors/Awards for the PI

Fellow of the American Physical Society
Fellow of the Optical Society of America

SEDSAT Final Report

Summary

Under this contract the Students for the Exploration and Development of Space Satellite number One (SEDSAT-1 or just SEDSAT) was completed and launched on 24-Oct-98. It achieved nominal orbit and activated its transponders after Delta II separation. Telemetry has indicated the internal systems are normal. However, SEDSAT has not responded to subsequent uplink commands. Telemetry has continued to be received allowing evaluation of bus performance and attempts at anomaly resolution. Anomaly resolution will continue during 1999 subsequent to the end of this contract. This final report documents activities under the contract period.

SEDSAT-1 Mission Description and Objectives

The SEDSAT-1 is the NASA/University of Alabama Huntsville Students for the Exploration and Development of Space satellite number 1. The purpose of the satellite is to advance the space education mission of the university and NASA, train students in a hands-on mission environment, and conduct science and engineering research.

SEDSAT Mission Objectives

The technical objectives are to demonstrate the implementation of advanced electronics, power systems, communications, and control algorithms; and perform remote sensing experiments; within the context of a student centered program of development and education. The high quality free remote sensing experiments were designed to take pictures of the earth after the satellite is ejected from the Boeing/McDonnell Delta II rocket. All the information is being placed on World Wide Web servers. The satellite (if/when fully operational) will provide services to the international amateur radio community.

The operational sequence for the satellite is:

1. Separation from the Delta II rocket
2. SEDSAT-1 automatically boots and takes a sequence of images as it separates from the Delta II. It immediately begins to attempt ground communication.
3. Once communications is established, the Delta II images are downloaded and the flight software is uploaded.
4. On command, the stowed antennas are deployed and full operational capability is established.

Communications

SEDSAT-1 will operate as a worldwide amateur radio communications link. The American Radio Relay League (ARRL) and the Radio Amateur Satellite Corporation (AMSAT) will provide tracking information and data acquisition/relay.

SEDSAT-1 will also provide a test bed for new forms of integration of scientific communication with the Internet. In the baseline configuration SEDSAT-1 will archive all of its telemetry and downloaded imagery through the World Wide Web. In a planned experiment, SEDSAT-1 will become a full-fledged Internet node accessible in real-time (albeit intermittently) directly through the Internet.

Earth Remote Sensing

The SEASIS imaging system objectives are to measure the planetary cloud cover, lightning distribution, and the diffusion of light by the Earth's atmosphere.

Technology Development

SEDSAT-1 will test new technologies in batteries, power management architectures, and high power in-situ processing of remote sensing data. Data will be collected on the on-orbit performance of the Marshall Space Flight Center supplied NiMh batteries. Power management will be distributed, utilizing local power conversion. The mass memory technology will be evaluated for space performance. Lastly, the control algorithms are new in the context of this application, magnetorquer control of a symmetric satellite.

Launch Considerations

SEDSAT deployment is controlled entirely by the Delta II. SEDSAT is non-operational during the entire ascent sequence. After the primary payload, Deep Space-1, is deployed the Delta II second stage performs a depletion burn. The second stage is commanded to the deployment attitude and is then commanded to release SEDSAT by activating the Marmon clamp pyro-cutters. The nominal SEDSAT release is at 5000 seconds when the second stage comes into view of the Hawaii tracking station near the end of the first orbit. Separation springs provide the energy to move SEDSAT away from the second stage. As SEDSAT moves away from the second stage the separation switches close and SEDSAT activates.

HARDWARE DESCRIPTION

The SEDSAT-1 hardware consists of the satellite structure, internal satellite subassemblies, body mounted GaAs/Ge solar arrays, and an integral Marmon clamp payload interface.

SEDSAT-1

SEDSAT-1 is a micro-satellite that consists of four major subsystems. These are the structure subsystem, launch vehicle interface subsystem, electronic assemblies and power subsystem, and the experiment subsystem.

SEDSAT-1 Structure

SEDSAT-1 has a design flight weight of 80 pounds. The satellite is a 13.65 X 13.65 X 12 inch near cube. Materials for the structure were bought from the approved list of structural materials and conform to MSFC-SPEC-522B "Design Criteria for Controlling Stress Corrosion Cracking." The materials used are listed in UAH-SEDSAT-0400. Materials selection was with the original intention of flying as a Hitchhiker payload on the space shuttle.

Five sides of the satellite are 1.27 cm (.5") 6061 T651 aluminum. The sixth side, which is the launch vehicle interface, is 7075 T73 aluminum to comply with the expected loads associated with the Marmon clamp. Figure 3.1.1-1 is a cutaway of SEDSAT-1 with the -X face removed showing the internal components.

SEDSAT-1 will be flown as a secondary payload on a Delta II launch vehicle. SEDSAT attaches to the secondary payload ejection system on the upper portion of the Delta second stage. The position of SEDSAT-1 on the Delta with respect to other structures is shown in figure 3.1.1.-2.

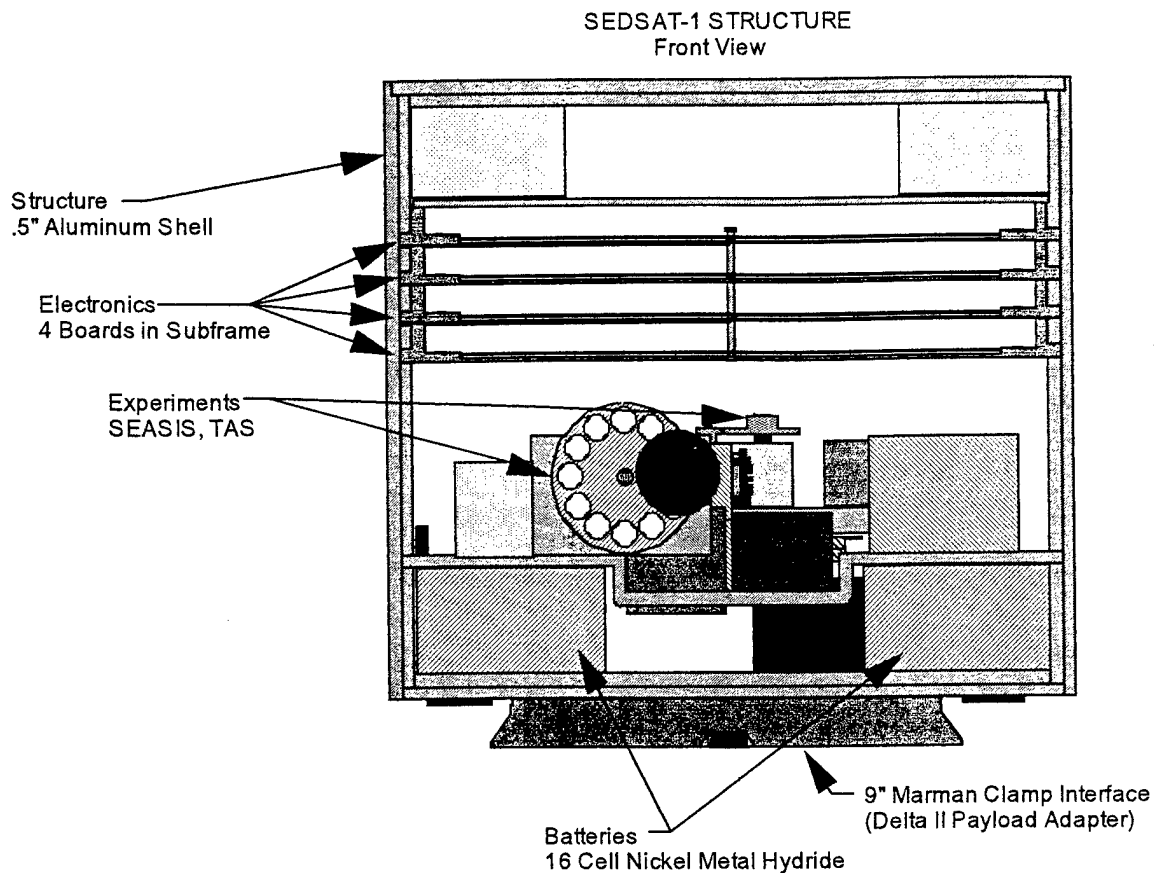


Figure 3.1.1-1 SEDSAT-1 Internal Hardware Placement

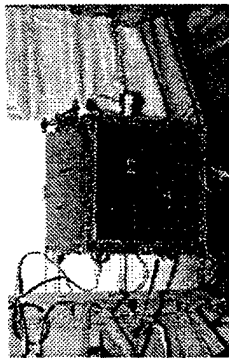


Figure 3.1.1-2 SEDSAT-1 on Delta II before fairing attachment

SEDSAT-1 External Configuration

Five of the six SEDSAT-1 surfaces contain GaAs/Ge solar arrays. They were constructed by TRW and Applied Solar Energy on a structural substrate provided by UAH.

The bottom (sixth side) of the satellite is the ejection system interface, consisting of a 9" Marmon Clamp. This interface was fabricated as an integral part of the bottom of the satellite to improve structural margins and is mechanically compatible with the Delta II Payload Adapter (PA).

The -X face of the satellite has only one protuberance, the SEASIS panoramic imaging camera lens and mount. Figure 3.1.2-1 shows external views of SEDSAT-1 with dimensions.

TBD Insert##

Figure 3.1.2.1 SEDSAT-1 External View (Antennas Not Fully Shown)

SEDSAT-1 Marmon Clamp Interface

Boeing Defense and Space constructed the Marmon clamp interface per original drawings from the McDonnell Douglas Corporation. The materials used conform to the applicable MSFC and GSFC requirements. The Marmon Clamp payload interface was designed as an integral unit as shown in Figures 3.1.3-1 and Figure 3.1.3-2.

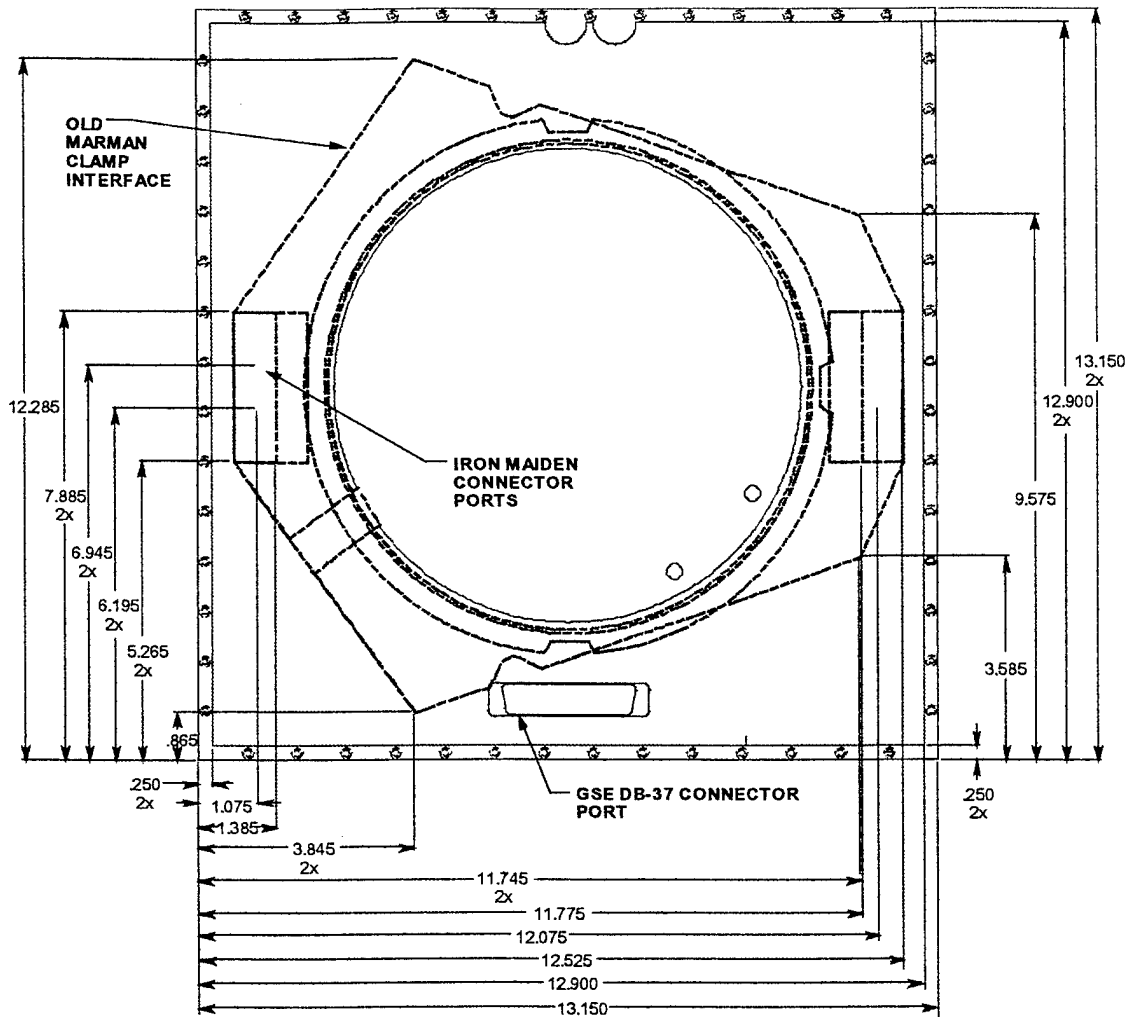


Figure 3.1.3.1 SEDSAT-1 Bottom and Launch Vehicle Interface (top view)

The original Marmon Clamp Interface utilizing a separate payload adapter is outlined within the above plate to illustrate where it would be in relation to the rest of the plate.

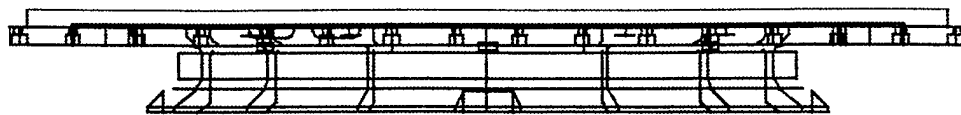


Figure 3.1.3.2 SEDSAT-1 Marmon Clamp Interface (side view)

Not shown in this drawing are the two physical plunger switches that protrude downward and contact the Delta II PA interface. Those switches can be seen clearly in figure 3.1.2-1. The switches are Honeywell commercial 1HE1-6 separation switches procured by NASA Marshall Space Flight Center. These switches

were originally designed for Mil-Std-8805. The two switches used on SEDSAT are the two passing members of a set of five subjected to a acceptance test in accordance with the acceptance test requirements of McDonnell Douglas Astronautics drawing 1B99614, Switch, Plunger, 4PDT.

Thermal System

The SEDSAT 1 satellite thermal system is passive. It is radiatively cooled during orbital operations and is passive while attached to the launch vehicle. All internal components are conductively cooled with thermal paths from heat generating elements to the external shell of the satellite. Thermal excursions during orbit are minimal because of the large thermal mass of the satellite and the concentration of that mass in the aluminum structural components.

There are four relatively "hot" spots on the satellite. These are the power amplifiers for each transponder, (two total) and the two antenna deployer thermal actuators. The two transponder power amplifiers have dedicated extra copper heat dissipation paths to the -Y/+Y faces of the satellite. The two thermal actuators are isolated from the satellite to reduce the total heat necessary to actuate during the deployment of the mode-A transponder transmit antenna. The batteries are not considered an important thermal source or sink due to their high efficiency and intimate contact with the -Z face of the satellite, which is the principal radiative face of the satellite.

During launch the satellite temperature is not controlled. The satellite is designed to be safe and operable throughout the temperature envelope of waiting for launch. The temperature excursions during launch were analyzed by Boeing and are documented in A3-L262-LEPT-98-134. The thermal excursions were very small compared to the designed operating range. The maximum temperature estimated was less than 75 deg. F.

SEDSAT Experiment Mounting Plate

The science experiments are mounted in a separate subassembly called the Experiment Mounting Plate (EMP). This plate is structurally independent from the rest of the satellite until final assembly. Figure 3.1.5-1 and 3.1.5-2 show the locations and arrangements of the SEDSAT-1 Experiment Mounting Plate subassembly.

When the EMP is integrated it acts as a structural stiffener. The EMP is 13.15" in the X or long direction. This provides a .25 inch inset into the -X, +X faces of the satellite. The -X and +X faces of the satellite have matching insets.

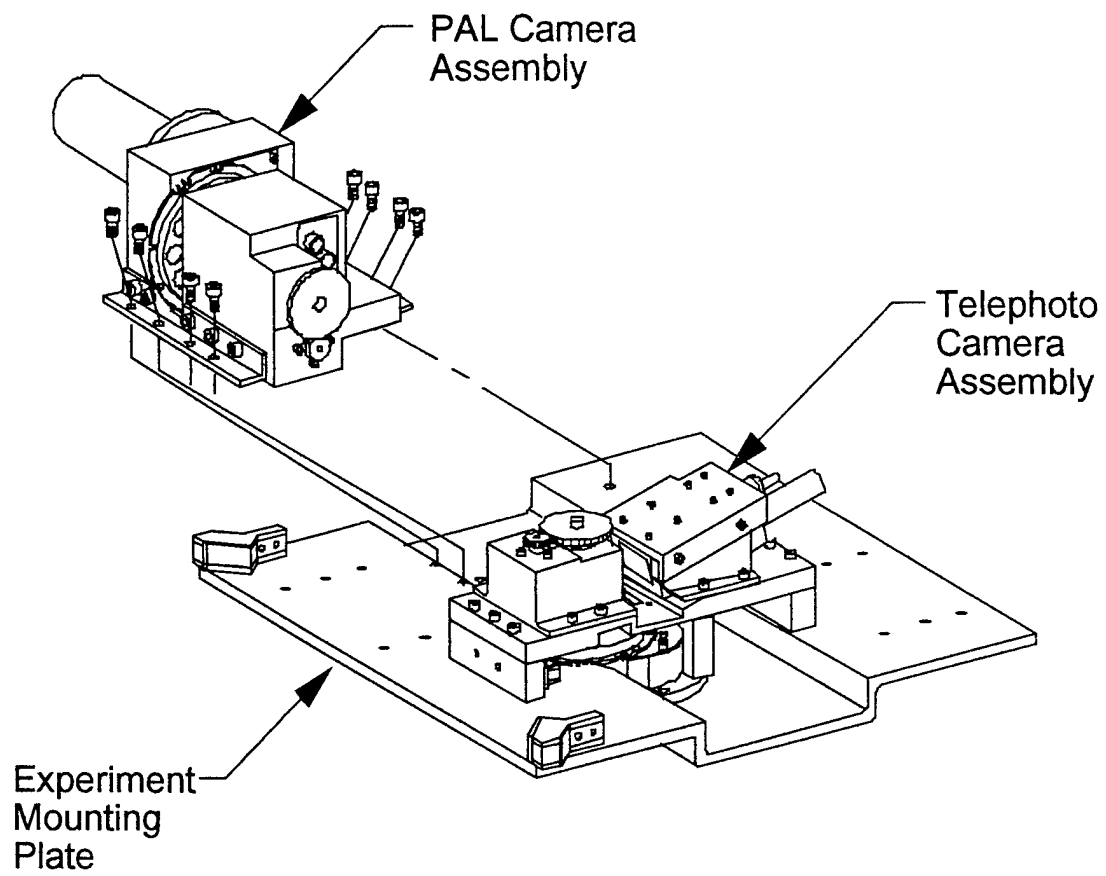
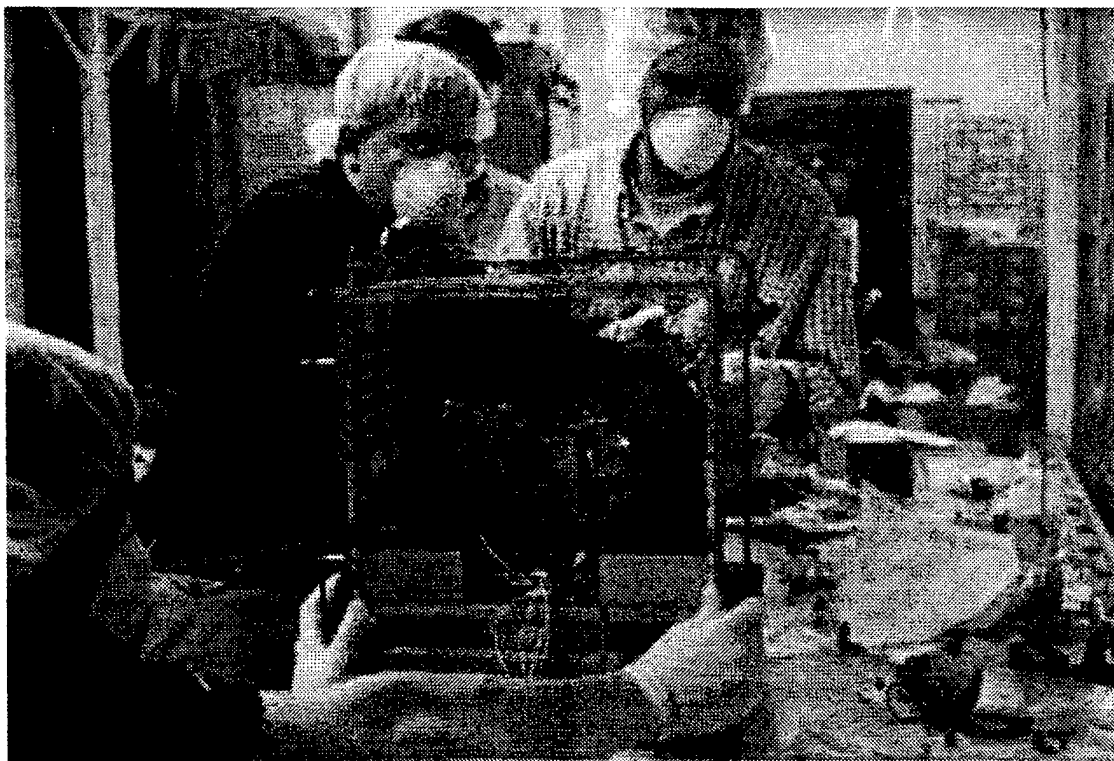


Figure 3.1.5-1 SEDSAT-1 Experiment Mounting Plate Subassembly



SEDSAT-1 Electronics Subassembly

The SEDSAT-1 electronics subassembly was designed to minimize the number of internal wiring harnesses. The electronics subassembly consists of five printed circuit boards. The top board is the mode A transponder. The second board is the Mode L transponder. The third board is the Command Data System. The fourth board is the SEASIS processor and mass memory board. The fifth is the motherboard. This board acts as the interconnect path between the four other boards. It also acts as the main path for distributing power to the other boards from the batteries and solar arrays. The electronics subassembly is attached to the main structure by wedge locks located on the Y face sides of the boards. Figure 3.1.6-1 is the layout of the subassembly.

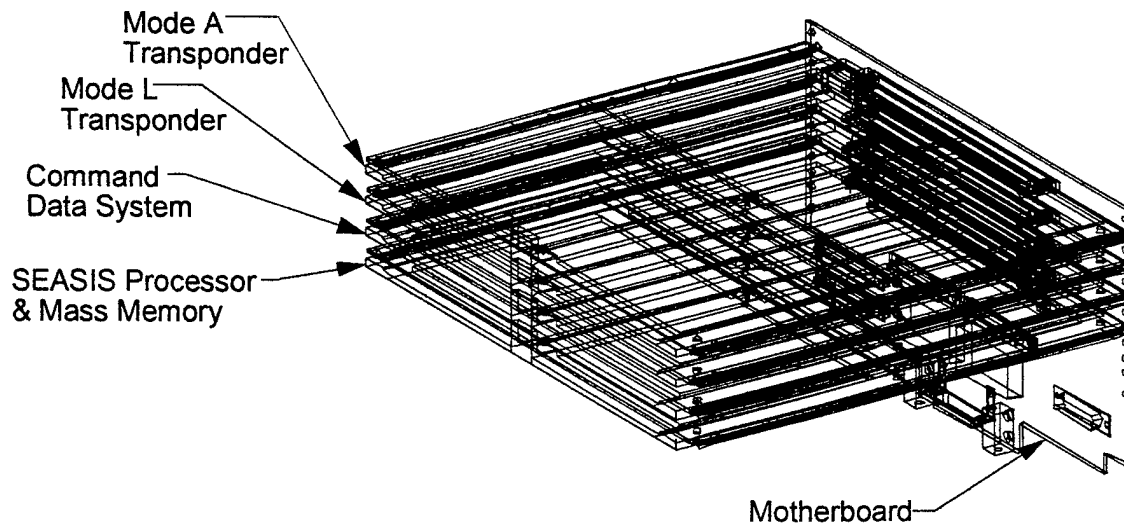
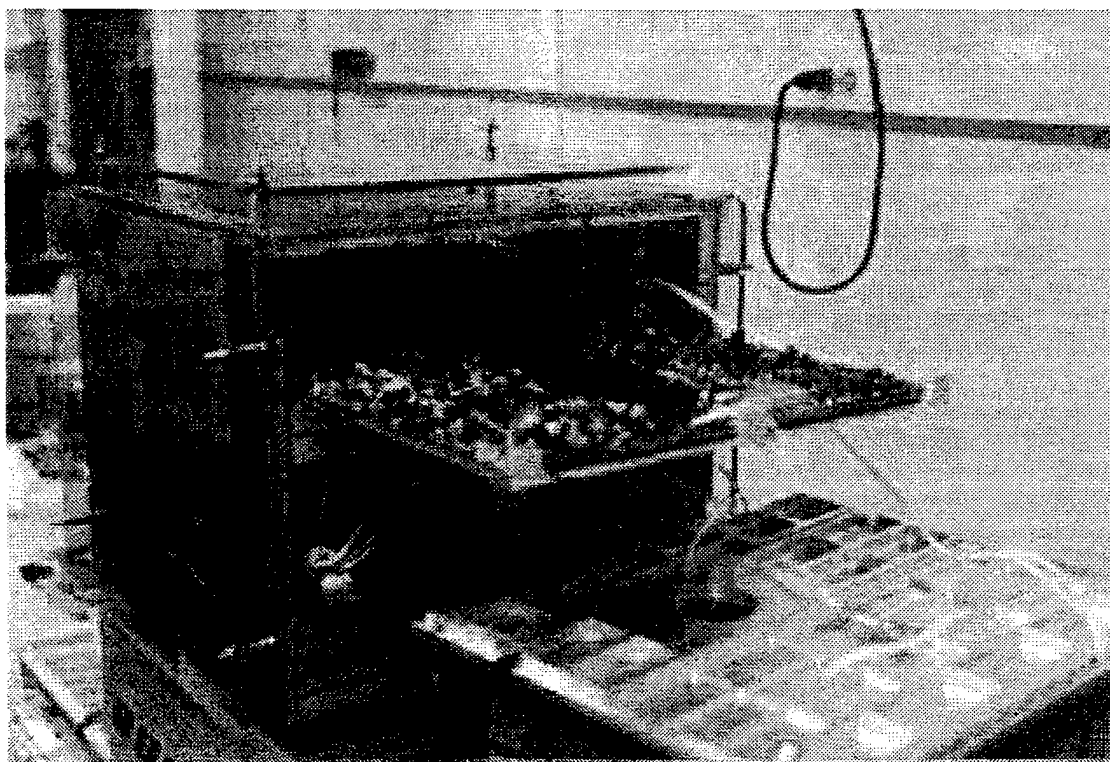
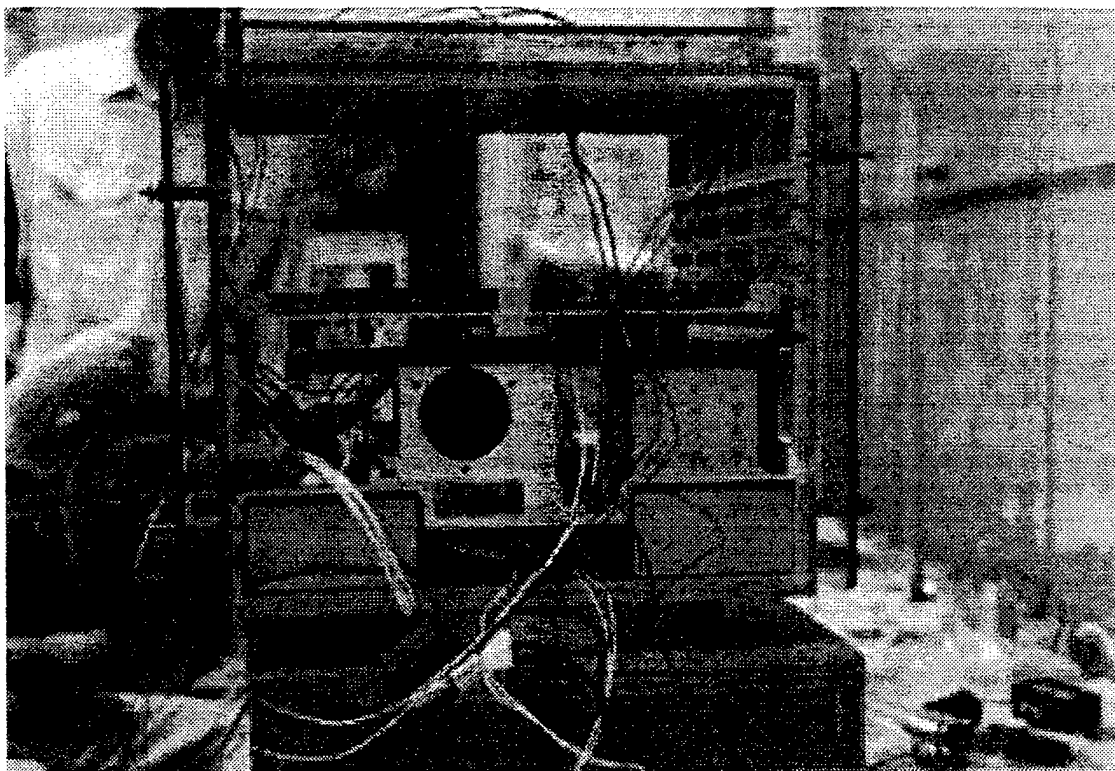
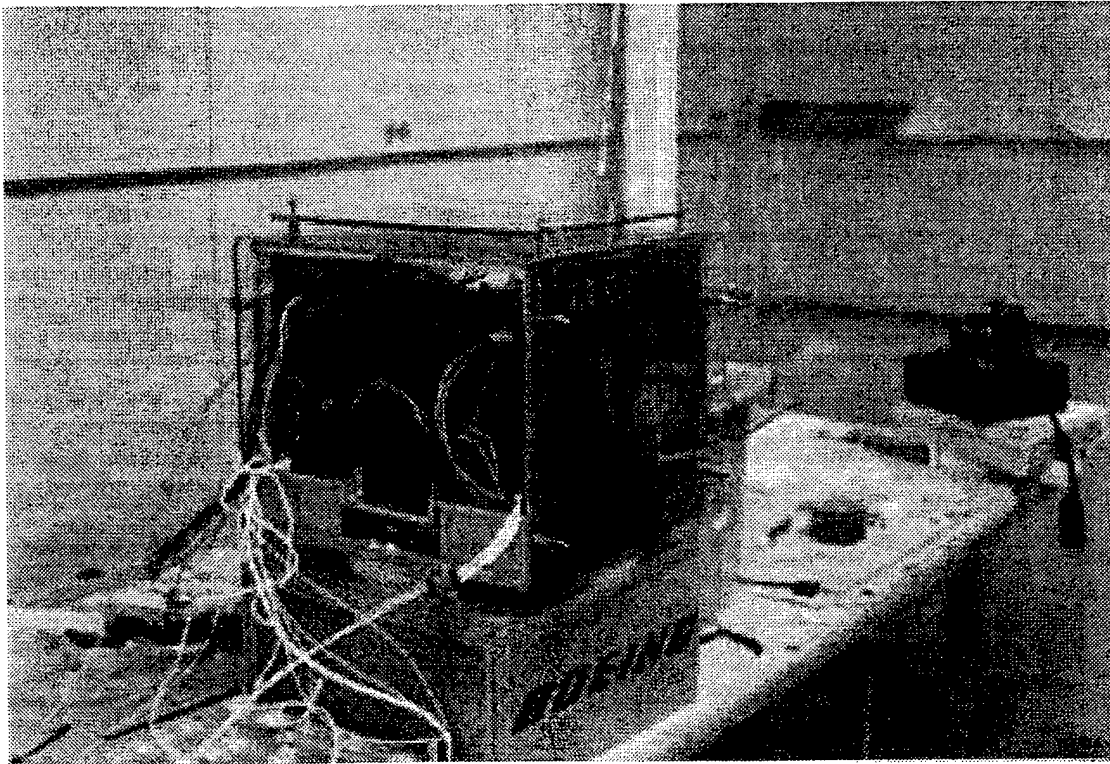


Figure 3.1.6-1 Electronics Subassembly Board Layout

The Electronics subassembly adds to structural stiffness through its installation. The motherboard is fastened across the Y axis elements. The wedge locks provide a thermal path from the multilayer printed circuit boards. The circuit cards ends opposite from the motherboard are inset into the main structure 0.25". All boards are attached to aluminum stiffener frames that also provide additional thermal contacts.





SEDSAT-1 Antennas

There are two sets of antennas (Mode-A and Mode-L) on SEDSAT-1 comprising a Mode-L transmit, Mode-L receive, Mode-A receive, and Mode-A transmit pair to support amateur radio satellite communications. The 70 cm wavelength (6 inches long) transmit monopole, the 2 m wavelength (19 inches long) receive monopole, the 23 cm wavelength (2.56 inches long) receive monopole, and the 10 m wavelength (8 feet long) dipole pair are all omni-linear antennas. Figure 3.1.6.1-1 shows the antenna configuration.

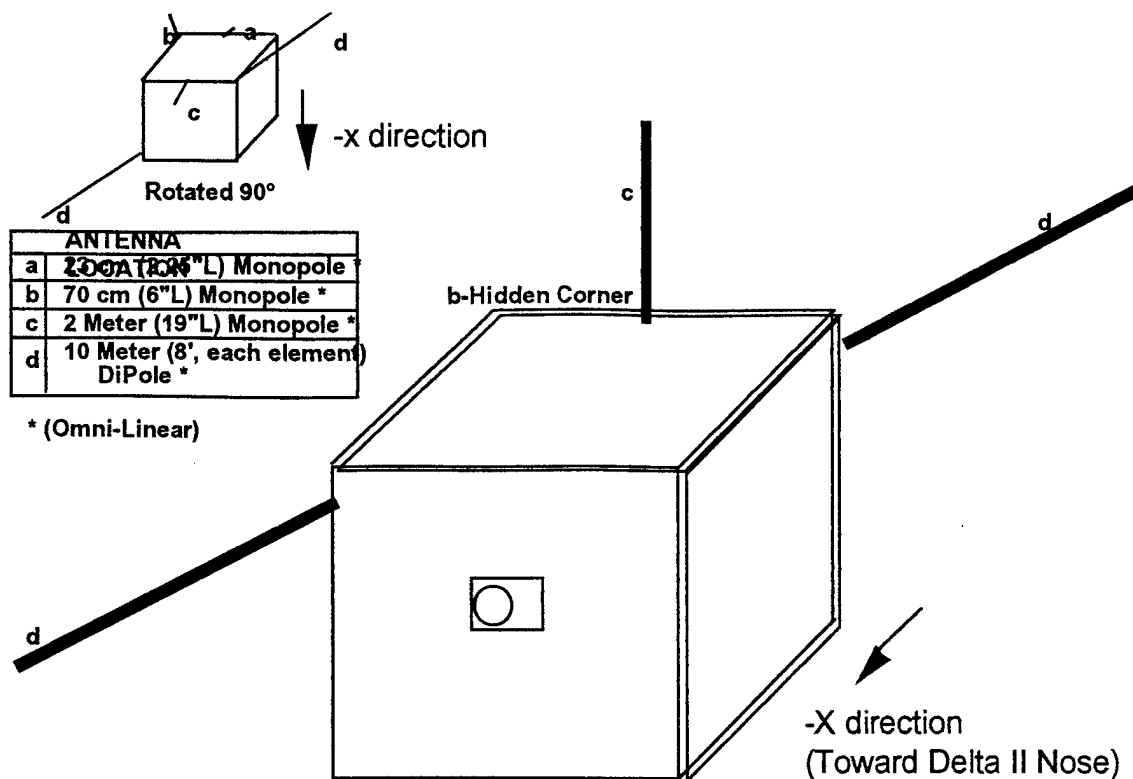


Figure 3.1.6.1-1 SEDSAT Antenna Configuration (After full deployment)

The antennas are made of spring steel from Stanley tape measures. This material is very common for use in Microsatellites. The table below gives details of the antennas.

Antenna Length (INCHES) and Weight (Pounds)

	Length (In.)	Weight (lb.)
a. 23 cm Monopole, Fixed	2.25	.1
b. 70 cm Monopole, Fixed	6	.05
c. 2 Meter Antenna, Monopole, Fixed	19	.1
d. 10 Meter Antenna, Deployed	96" each	.5

The fixed antennas are secured to the satellite by machined pieces of Delrin black with 440 metal fasteners.

SEDSAT-10 Meter Antenna and Deployer

The only deployable antennas on SEDSAT-1 are the two 10 meter band antennas. The antennas are each 96" in length and are made from the same Stanley tape measure material as the fixed antennas. After the satellite is deployed from the Delta II and is in its final orbit, the antennas will be deployed. The antennas are stored furled in the antenna deployers, held in by a swinging door that is prevented from moving by a latch. The latch is rotated open by thermally activated actuators. After the door opens each antenna will deploy from the force of its own spring tension.

The actuators are a thermal paraffin type that has a stroke of approximately 0.4 inches. The paraffin is heated to its melting point by a Kapton Insulated Flexible Heater. The melting paraffin expands, pushing the actuator piston its stroke distance. The process of heating the paraffin to a temperature hot enough to cause the actuator to travel its stroke length takes approximately 10 minutes at a heater current of 1 amp. The part is made by Actronics Incorporated and the part number is P/N 11-546. This actuator has been designed into other NASA missions and the certification of compliance with NASA and military standards

are on file at NASA MSFC and UAH. The specified actuation temperature is no movement below 180 deg F and full stroke at 195 deg F.

The antenna deployment mechanisms are located within the top two inches of the satellite. They are mounted on a .125 " thick plate that is located above the electronics subassembly. Figure 3.1.6.2-1 shows the placement of the antenna canisters on the mounting plate.

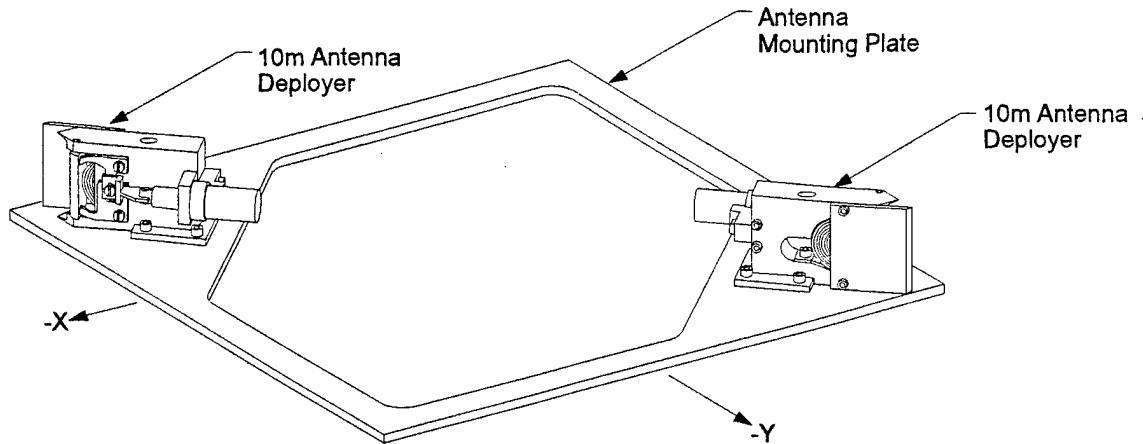


Figure 3.1.6.2-1. Antenna Mounting Plate With Antenna Deployers

The weight of the antennas is 0.067 lbs. each. The closing force of the deployer doors is 1.52 Newtons. The antenna deployers receive power from the main power bus through an Interpoint DC/DC converter and a bank of power MOSFETs, which are controlled by a CDS controlled multiplexer. The deployers are powered on by the CDS board activating the DC/DC enable through software and selecting the deployer power MOSFET through the mux. In order to activate the deployers the satellite must power on (which is inhibited as described below) and the CDS provided converter enable and mux signals must go high. The schematic is shown in figure 3.1.6.2-1. The deployers, like other onboard electronics, are not monitored on the ground because they are unpowered.

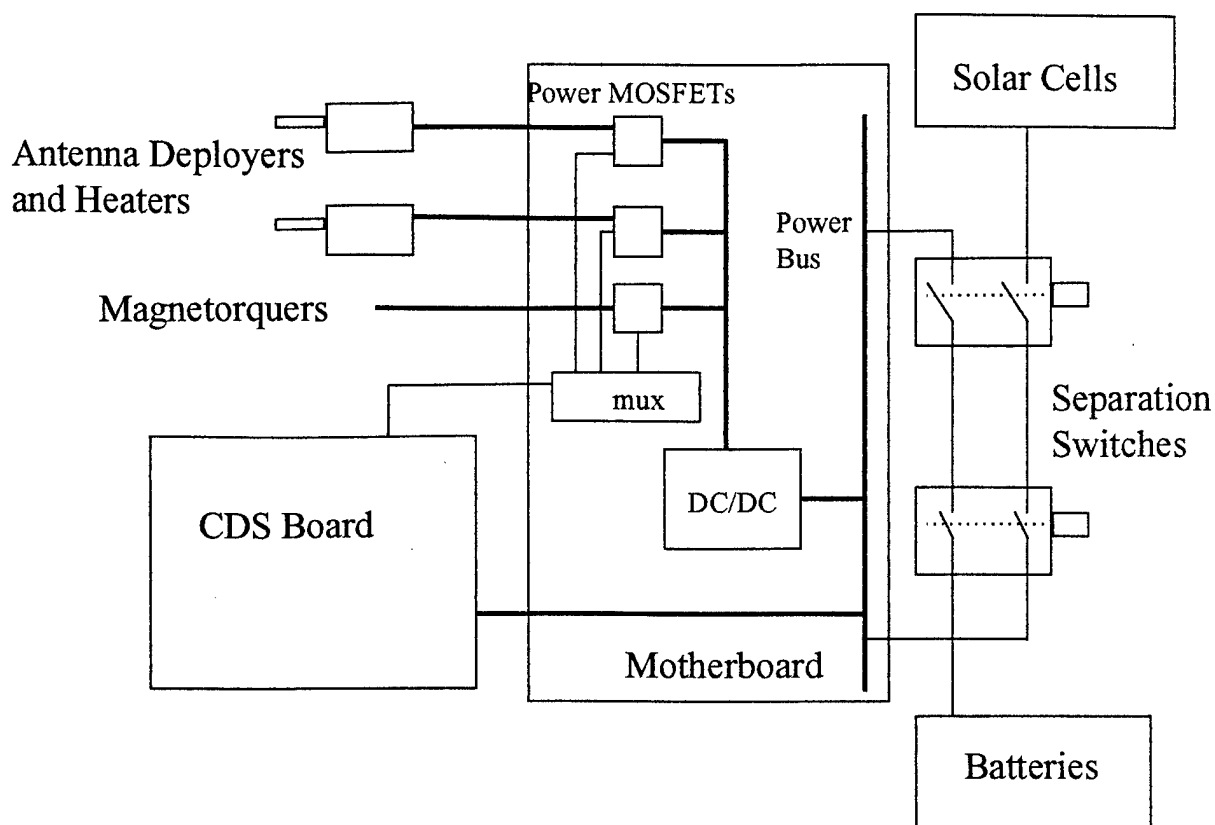


Figure 3.1.6.2-2. Antenna deployer schematic

SEDSAT-1 Electrical Power System

SEDSAT-1 does not have a centralized power regulation system. Each subsystem has its own DC/DC converter to power its functions. The layout of the power system is shown in figure 3.2-1. This figure also shows the terminals available at the GSE ports, allowing verification of the status of the separation switches, external battery charging, and enabling and disabling of the satellite. There are a total of six Interpoint DC/DC converters used in SEDSAT-1. With a wide input range (16 to 40 volts) these converters regulate to within 1% of stated output voltage. Several advantages to this design are:

1. Simplified power supply design. (No central custom supply to build)
2. Simplified wiring harness. (Only main power distributed)
3. High Efficiency DC/DC converters space qualified and available inexpensively.
4. DC/DC converters incorporate power inhibits to simplify power control.
5. Some fault tolerance to subsystem overcurrent failures since individual DC/DC converters can isolate the remaining subsystems.

The schematic of the power distribution system is shown in figure 3.2-1 and is further described herein. Inadvertent power on of hazardous subsystems is prevented by two means. First, power is redundantly inhibited through the separation switches once the PAF is attached. Second, power is inhibited by safety plugs (or by the lack of any plug) in the GSE ports during all handling during which the separation switches are allowed to close. While safety plugs can be used, the configuration of the GSE ports is such that the system is inhibited from powering on unless flight jumpers are inserted. The basic safety strategy is to keep the system unpowered until flight separation. In addition, the system can only be commanded to perform some hazardous operations (such as antenna deployment) by a relatively complex communications protocol.

While in an unpowered state with the batteries fully charged there is a potential shock or sparking hazard at points that are battery energized. These hazards are ameliorated through a variety of design practices. Since GSE port pins are powered, the GSE port connectors are female only. Internally, powered sections are in close proximity only at the separation switches, which are hermetically sealed.

The RF radiation hazard is inhibited only by keeping the spacecraft in an unpowered state. If the separation switches are allowed to close while a flight jumper is in place the system will begin to radiate, and will not give any external indication that it has done so. This issue is controlled by monitoring the state of the separation switches via electronic measurement during and after PAF installation and at any other time until the flight jumper is installed. The flight jumper is installed on only one GSE port. It is possible to monitor the spacecraft from the other GSE port at any time, but only by attaching a cable and GSE (the switch/fuse box) to the satellite.

The numbered terminals in figure 3.2-1 ### redundantly map to the GSE port pins. The pin mappings for the GSE ports and the plugs used are shown in Table 3.2-1.

Port A		Port B		Flight Jumper	
Pin Number	Fig 3.2-1 Terminal	Pin Number	Figure 3.2-1 Terminal	Port A	Port B
1	1	1		2 to 3	2 to 3
2	9	2	7		6 to 7
3	10	3	8		4 to 5
4	4	4	2		8 to 9
5	5	5	1		
6	6	6	7		
7	7	7	8		
8	3	8	2		
9	8	9	1		

Table 3.2-1: GSE Port pin mapping

The charging plug brings all Port-A pins to the switch/fuse box. Current is applied to pins 1 and 9 (corresponding to terminals 1 and 8).

Electrical Power System and the Interface to the Delta II

There is no electrical interface between SEDSAT-1 and the Delta II rocket. SEDSAT-1 electronics are unpowered until deployment. The batteries are charged and the solar cells may be active, but power from both is inhibited from the electronics by the separation switches. The separation switches are single pole, dual throw plunger switches (Honeywell part 1HE1-6). Each separation switch incorporates two isolated, single pole, dual throw switches actuated by a common plunger. The plunger seats on a spring that provides enough force to extend the plunger. When the plunger is extended one of the switch poles is engaged. When the plunger is compressed the switch pole is disengaged, and the opposite pole is engaged when plunger travel is nearly complete. SEDSAT uses two of the Honeywell switches connected in series to provide single fault tolerant inhibiting of the SEDSAT electronics. The separation switches are mounted inside the Marmon clamp ring with the plunger protruding below the interface ring (shown in figure 3.2.1.3-1). When SEDSAT is mated to the payload attach fitting (PAF) the separation switch plungers are pressed against the surface of the PAF. The switches are mounted so that the plunger depression against the PAF is nearly equal to full travel.

Only the plunger extended switch pole is used on SEDSAT. The depressed pole is often used in other applications of the Honeywell switches, but is not used on SEDSAT. The plunger extended poles are wired into the SEDSAT electronics.

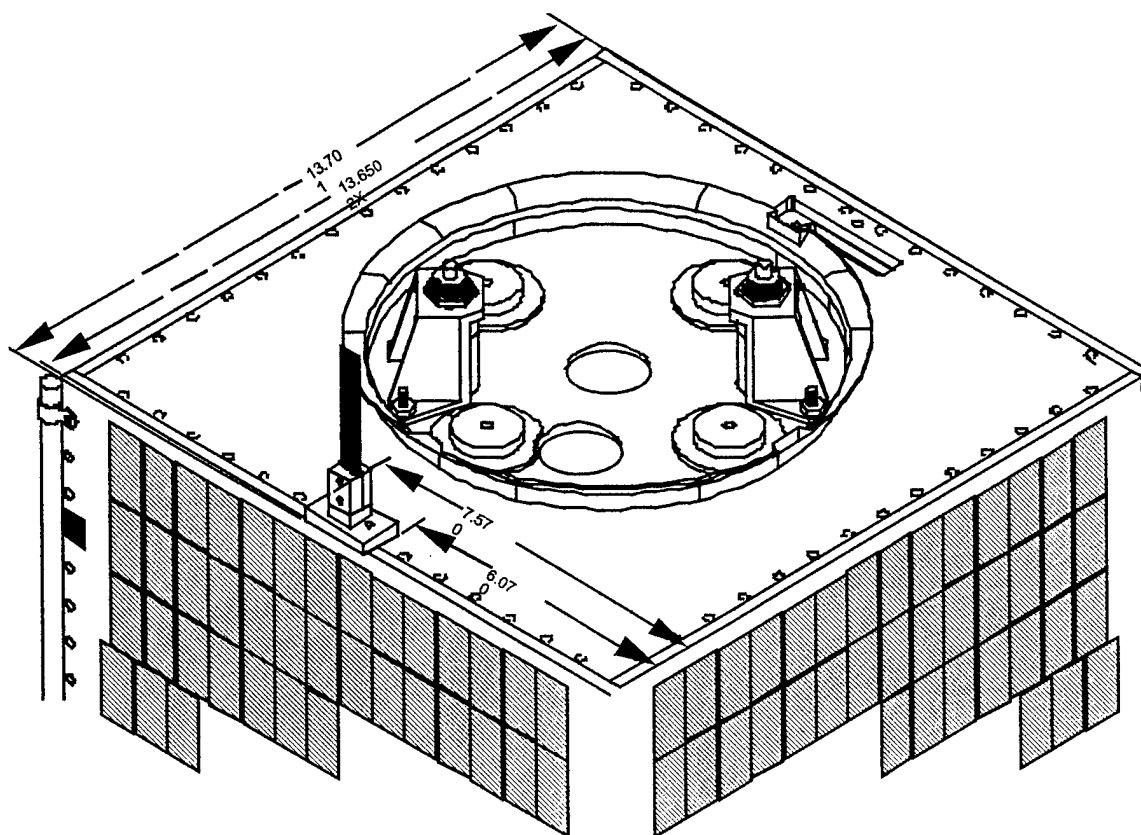
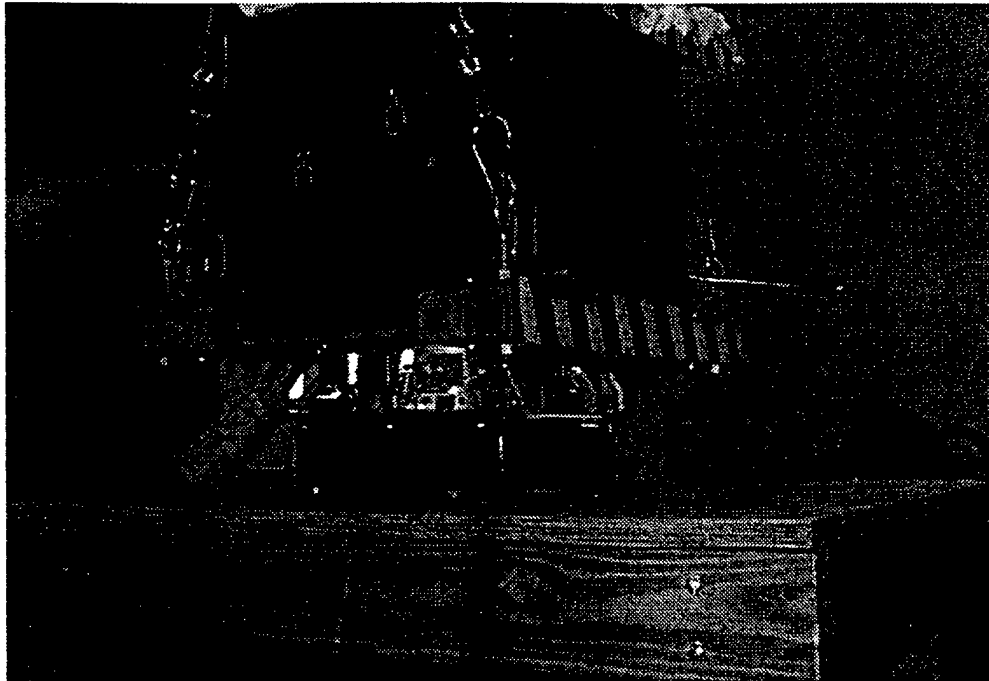


Figure 3.2.1.3-1 Separation switches on -Z face plate

Electrically, the switches disengage both the batteries and the solar arrays from the satellite. Battery positive and solar panel positive both pass through the two switches (in series) before reaching each other on the main power bus. Both separation switches must fail closed to allow power from either the batteries or solar panels to reach the electronics, or each other. The negative sides are separated from each other until the flight GSE plug is installed, and the main power bus is separated from the electronics by the same plug. This arrangement is shown in figure 3.2-1.

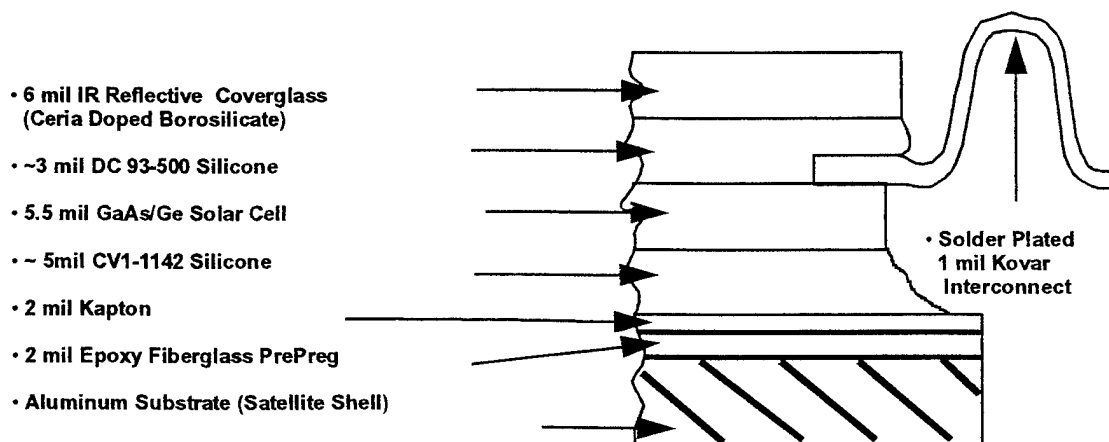
At the moment of ejection the plungers are released, and the switches move to the wired poles connecting power to the satellite. The arrangement of the power system with the physical switches is dictated by the Secondary Payload Planner's Guide for requirements for single fault tolerance to insure non-operation before separation. Figure 3.2-1 is the schematic for the separation switch inhibit mechanism. Also included is the GSE interface that allows the bypass of the switches for ground testing, verification of safety interlock operation, and charging of the batteries after closeout of the satellite structure.

The Honeywell 1HE1-6 separation switches were selected in a compromise between availability and qualification. Honeywell has previously supplied a separation switch built to a McDonnell-Douglas specification and built to a reliability program. Unfortunately, these switches are no longer manufactured and no alternate switch with a full qualification and reliability program will be offered in the foreseeable future. Instead the decision was made to use a hermetically sealed, Mil-8805 qualified switch put through the same acceptance test as called for in the previous McDonnell-Douglas specification. Of five 1HE1-6 switches put through this test program two passed. The three failing switches failed hermetic seal but did not fail in operation. The two passing switches are used on SEDSAT-1.



Solar Arrays

The solar arrays for SEDSAT-1 are GaAs/Ge arrays and were provided by TRW and Applied Solar Energy Corporation. On each of the five faces there are three strings with 32 cells in series on the TRW arrays and 35 cells per string on the Applied Solar Energy arrays. Each string is diode protected from shadow induced reverse currents by low loss diodes located on the motherboard. The wire gauge for each string is 26 and complies with appropriate Delta standards. The arrays were assembled on the SEDSAT-1 structure to reduce manufacturing costs and pointing requirements for the arrays. Figure 3.2.1.4-1 shows the solar arrays and how they are assembled on the satellite structure.



TRW Supplied Arrays

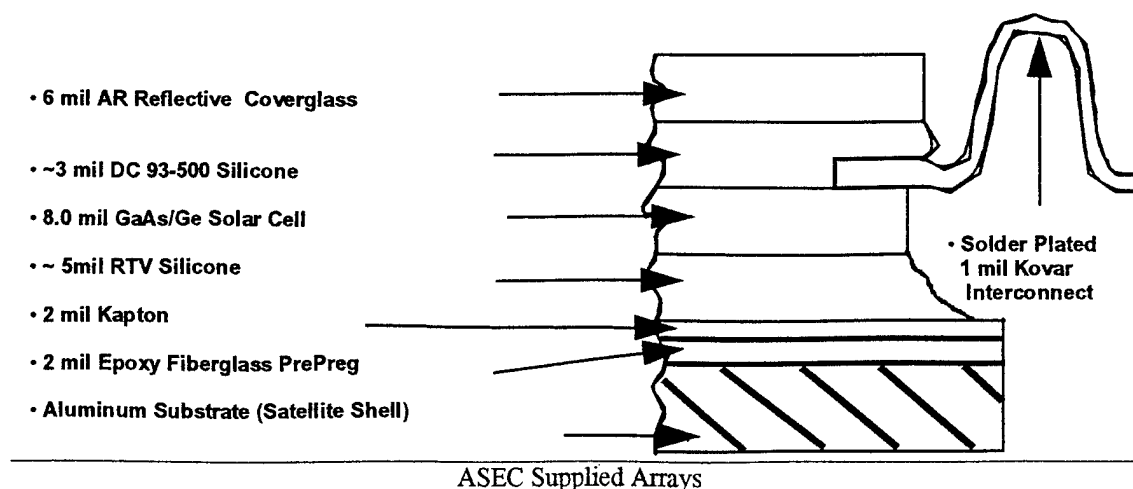


Figure 3.2.1.4-1 SEDSAT-1 Solar Array Materials and Construction

The coverglass for the solar arrays comprise two different types. The TRW supplied solar arrays, (+Z, +/- Y faces) use an IRR coverglass material that is reflective in the infrared and will work to lower the temperature of the solar arrays and the satellite. The Applied Solar Energy supplied solar arrays use the standard CMX coverglass.

Battery

The SEDSAT-1 battery is the source of energy to operate the satellite during the shadow portion of the orbit. The batteries use 8 Ah Nickel Metal Hydride (Ni-MH) cells. There are 16 cells total with eight cells packed into each of two battery boxes. The cells are Nickel Metal Hydride chemistry containing 32 cc per cell of 1.3 specific gravity potassium hydroxide electrolyte. The battery boxes have two vent holes that also provide for routing of the wiring into and out of the box. A venting analysis including the effects of the wiring has been performed and shows less than .001 psi pressure differential during Delta ascent. Figure 3.2.1.5-1 illustrates the battery box design for containing the Ni-MH cells.

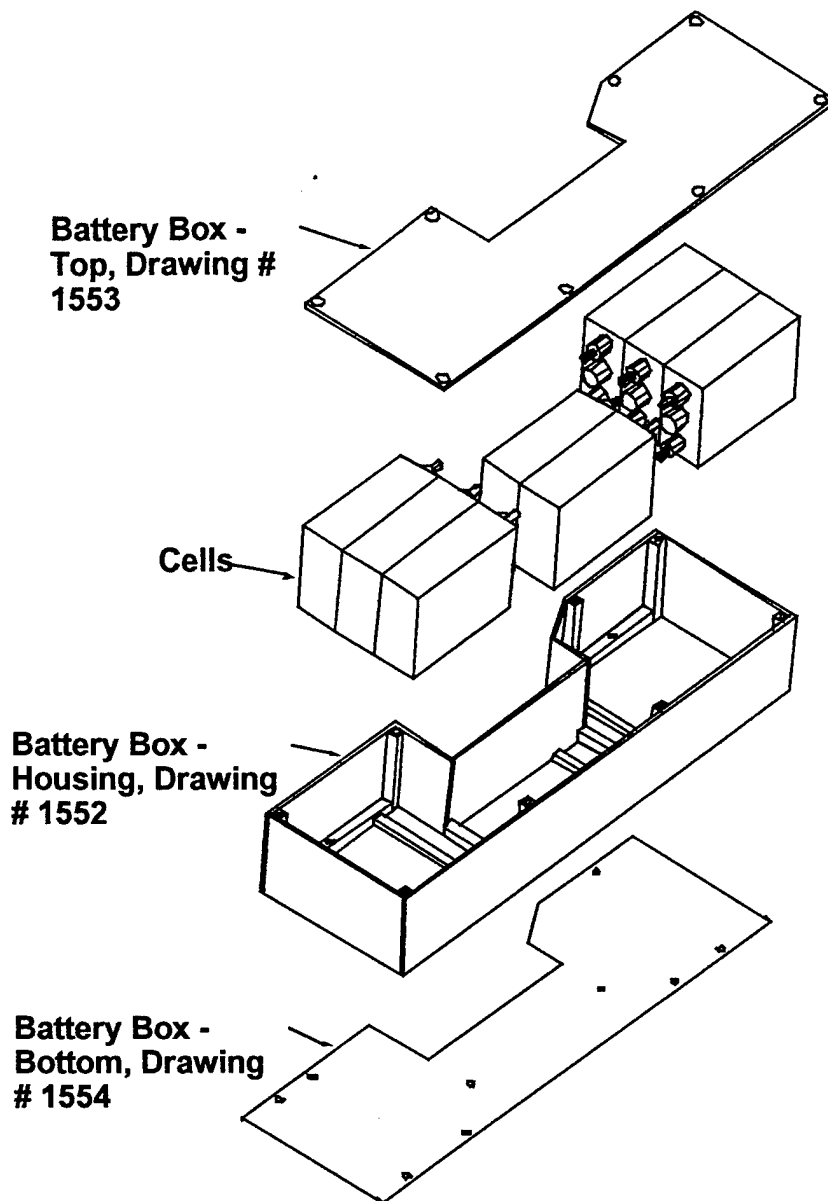


Figure 3.2.1.5-1 SEDSAT-1 Battery Box (2 each)

The cells themselves are prismatic cells with the same specifications as military standard NiCad cell prismatic packaging. These cells have a relief valve installed to vent in the event of severe overpressure. The valves operate at 180 psi +/- 20 psi. The burst pressure for these batteries is approximately 600 psi. Test information regarding failure of the battery has been obtained and can be provided through the MSFC battery laboratory. Figure 3.2.1.5-2 shows the construction of the cells used for the SEDSAT-1 battery, while figure 3.2.1.5-3 ### shows an external view of the cells.

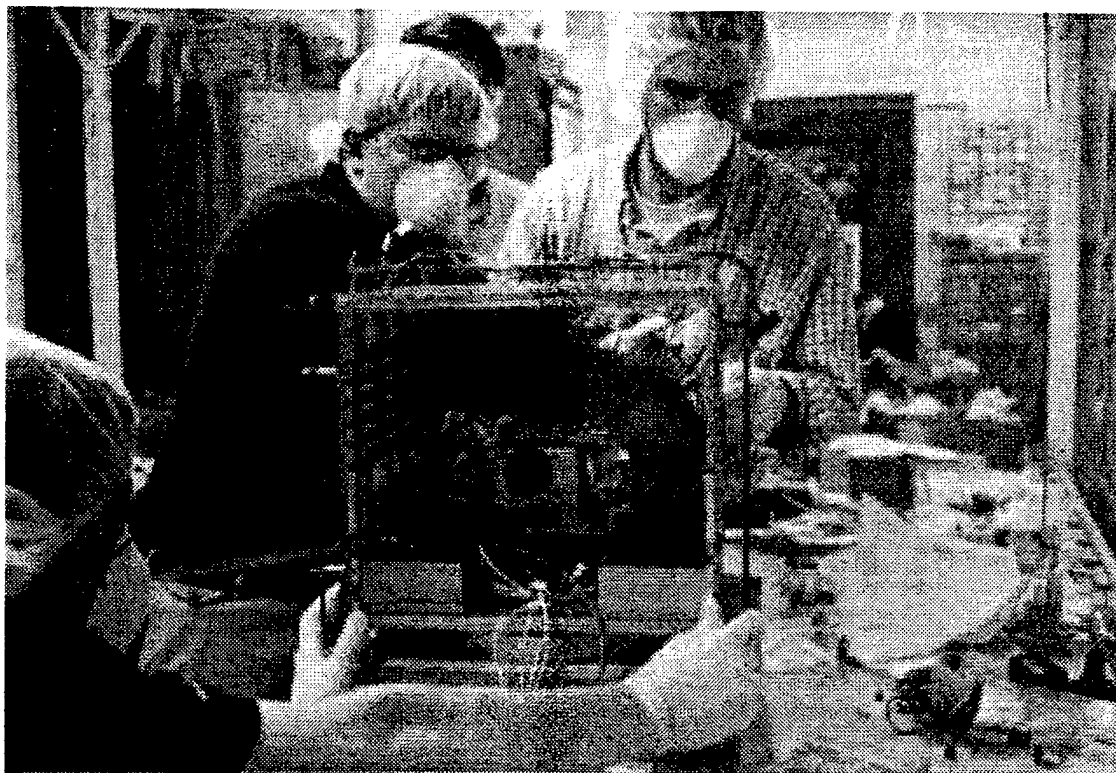


Figure 3.2.1.5-2 SEDSAT-1 Nickel Metal Hydride Cell

These batteries do involve a safety hazard and are covered in the safety section of this document and in a hazard report. One consideration for safety is the safety of trickle charging. Trickle charging is planned only for the SSPF and so does not involve hazards to the Delta II or primary payload. At the specified trickle charge level of 23 volts and current limited to 0.1 amps the batteries do not rise in temperature enough to pose a hazard. As an example, a duplicate set of flight batteries were trickle charged in an insulated container to and beyond full charge. The temperature history is shown in figure 3.2.1.5-3. Charger overcurrent is inhibited by manual setting of the charger power supply, by charger box fuses, and by monitoring.

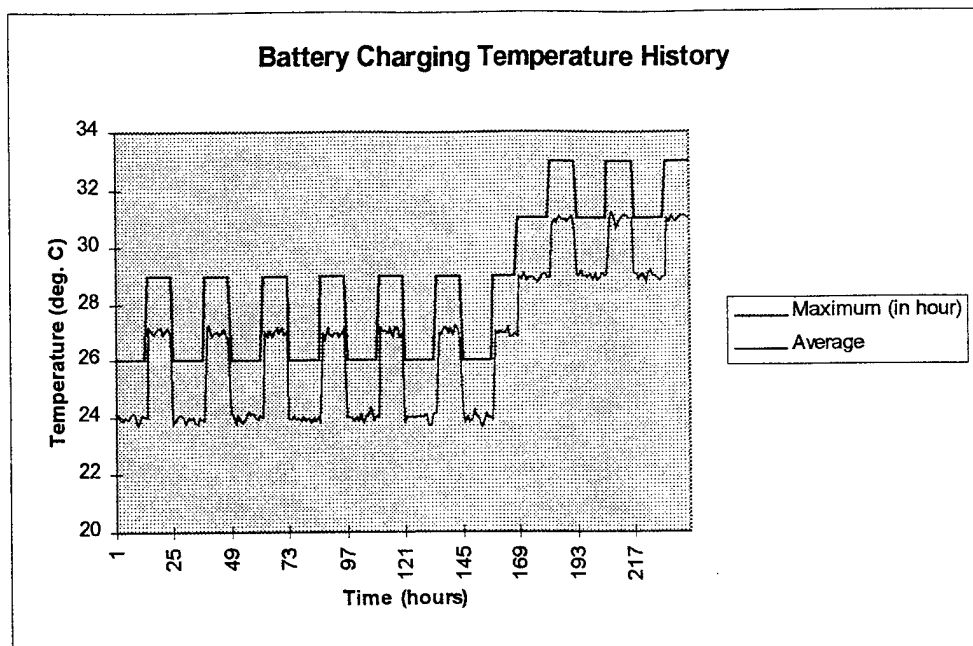


Figure 3.2.1.5-3 SEDSAT-1 Trickle charge battery temperature history

SEDSAT-1 Communications System

The communications system for SEDSAT-1 is intended for the use of amateur radio satellite operators worldwide and transmission of scientific data. There are two transponders on board. The primary transponder is a Mode L transponder as defined by the International Amateur Radio Union. The second is a Mode A transponder that will be used as a backup to the primary transponder. Table 3.3.1 gives the characteristics of the communications system and a summary link budget analysis.

Parameter	Mode-A (Analog repeater)	Mode-L (Digital)
Frequency		
Uplink	145.915 to 145.975	1268.175 to 1268.250
Downlink	29.35 to 29.41	437.850 to 438.000
Maximum power (EIRP)	10 W	5 W
Average power, W	8 W	3 W
Type of Transmitter	Class AB Linear	Class AB Digital
Antenna Gain	0	0
Antenna Location	+Z and deployed	-Z and XY side
When operated	On orbit after separation and software command (No RF on pad or SSPF)	Tests in SSPF, on orbit after separation (automatic), no RF on pad
Link Budget		
Nominal Range, km	1000	1000

Downlink rec. ant. Gain, dB	0	5
Downlink Received Power, dBm	-82	-103
Uplink Transmit power, W	10	10
Uplink Trans. Ant. Gain, dB	5	10
Uplink Received Power, dBm	-91	-104

Table 3.3.1 SEDSAT-1 Communications System Characteristics

Between delivery to Cape facilities for launch and orbital separation from the Delta II the only planned radiation will be during delivery acceptance tests, which are conducted in the SSPF. Inadvertent radiation is inhibited by removing the flight plugs from the GSE ports, and by the compression of the separation switches during PAF installation. Once the PAF is installed in the SSPF there will be no further radiations. The planned radiations will involve only the Mode-L transponder and will be performed only at the integration facilities (SSPF), not in the launch pad area. The required Radio Frequency Authorization and Use Authorizations have been submitted and approved.

Safety hazards associated with the SEDSAT-1 communications system are minimal. During ground operations the primary hazard is personnel exposure during planned radiation. Because of the low power of the system this hazard is easily controlled by maintaining adequate separation distances (specified distance is 1 meter). Radiation could pose RF interference hazards to other Delta II frequencies. This is controlled by the physical inhibits of the separation switches preventing the communication system from being powered on as long as the PAF is attached, which will be so throughout the flight until Delta II commanded separation. SEDSAT-1 will be unpowered and unable to radiate throughout launch operations. Figure 3.3-1 shows the curve of power density for the 5 watt transponder radiating from 0 dBLi antennas.

Link graph ##

Figure 3.3-1 Transponder power densities

Mode A Transponder

The mode A transponder is derived from the successful mode A transponders flown by AMSAT in the mid 1970's. The frequencies of operation and the system configuration is shown in Figure 3.3.1-1

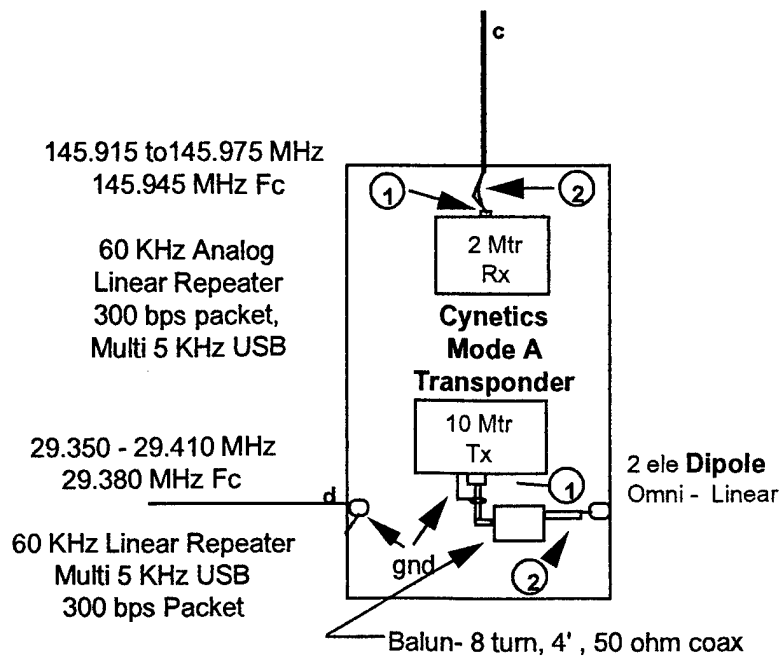


Figure 3.3.1-1 Mode A Transponder System Configuration

The uplink is in the amateur radio 2 meter band. The downlink is in the amateur radio 10 meter band. The primary use of this transponder is for voice communications between amateur radio operators within the RF footprint covered by the satellite. A secondary 300 bit per second data link that is compatible with terrestrial HF packet radio communications is included as a back up to the primary mode L transponder in the event of its total failure. This transponder will not be powered on during ground operations or while attached to the Delta II. The Mode-A transmit antennas will not be deployed until SEDSAT is ejected from the Delta II and Mode-L operations have commenced. The Mode-A transponder is not powered until after the satellite has been deployed into orbit, the antennas have been deployed, and additional software has been uploaded.

Mode L Transponder

The mode L transponder on SEDSAT-1 acts as the primary communications system for the satellite. The transponder communicates at a maximum data rate of 56 kilobits/sec. This will be the primary method of obtaining telemetry and experiment data from SEDSAT-1. Figure 3.3.2.1 outlines the frequencies of operation and configuration of the system.

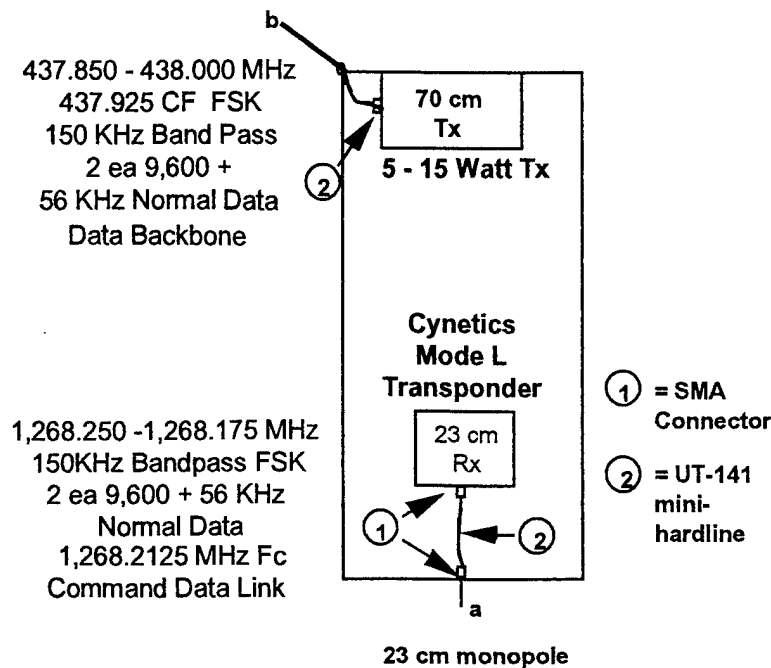


Figure 3.3.2-1 SEDSAT-1 Mode L Transponder System Configuration

After initial delivery tests are complete and the PAF is installed on SEDSAT, this transponder will not be active until SEDSAT is ejected from the Delta II. The transponder will be active during ground operations only during selected functional tests (for example, for a test after the vibration and shock tests). Operation of the transponder during test is described in UAH-SEDSAT-1803. A hazard report outlines hazards relating to the RF radiation of this system.

SEDSAT-1 Command Data System

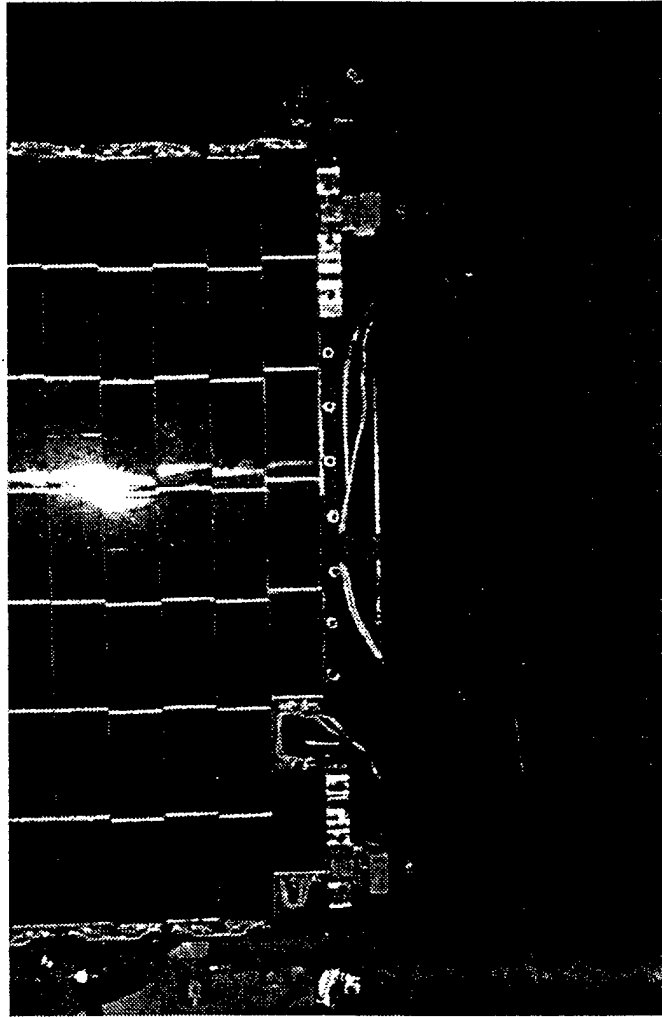
The Command Data System (CDS) will comprise the bulk of SEDSAT-1's control electronics. The command data system (CDS) design closely parallels the AMSAT UK UoSat design in order to retain as much software compatibility as possible. This design consists of an Intel 80C186 microprocessor, two Intel 82C530 Serial Communications Controllers (SCC's), 2 megabytes of 12 bit error detecting and correcting memory and 48 analog inputs to the A/D converters.

The objective of the Command Data System (CDS) is to serve as the command processor for SEDSAT-1. The functions that the CDS controls are as follows:

1. Command uploading of new programs from the ground.
2. Serial communications through the digital and analog transponders.
3. Electrical power system control.
4. Record telemetry from the TAS and SEASIS experiment.
5. Watchdog Timer for system reset on loss of software control.

Attitude Control System

Attitude Control of SEDSAT-1 is accomplished actively by the use of electromagnets controlled by the Command Data System. There are two sets of electromagnets. One set is aligned along the Z axis of the satellite and the other set is aligned along the X/Y axis. This system will not be enabled until SEDSAT has completely ejected from the Delta II rocket. After deployment, the system will be enabled and, over a period of about a month, nadir pointing will be established with the Marmon Clamp facing the Earth.



SEDSAT Experiments

SEASIS

SEASIS has two imaging subsystems that share processing and control electronics (Figure 3.6.1-1). The telephoto system has a telephoto lens with a 10 degree field of view that will be pointed nadir (or in the nadir direction) after SEDSAT has reached its final orbit. The Panoramic Annular Lens (PAL) imaging system will be pointed 90 degrees away from zenith or nadir. Both systems have a filter wheel which has 6 narrow band filters, 4 broad band filters, and 2 neutral density filters. They also have a Sony CCD camera that will capture the images focused onto the image plane by the lenses. SEASIS has redundant video digitizers that will digitize images from the cameras mounted on the Transputer based SEASIS processor/memory subsystem. The Transputer is the computer chip used for the SEASIS electronics.

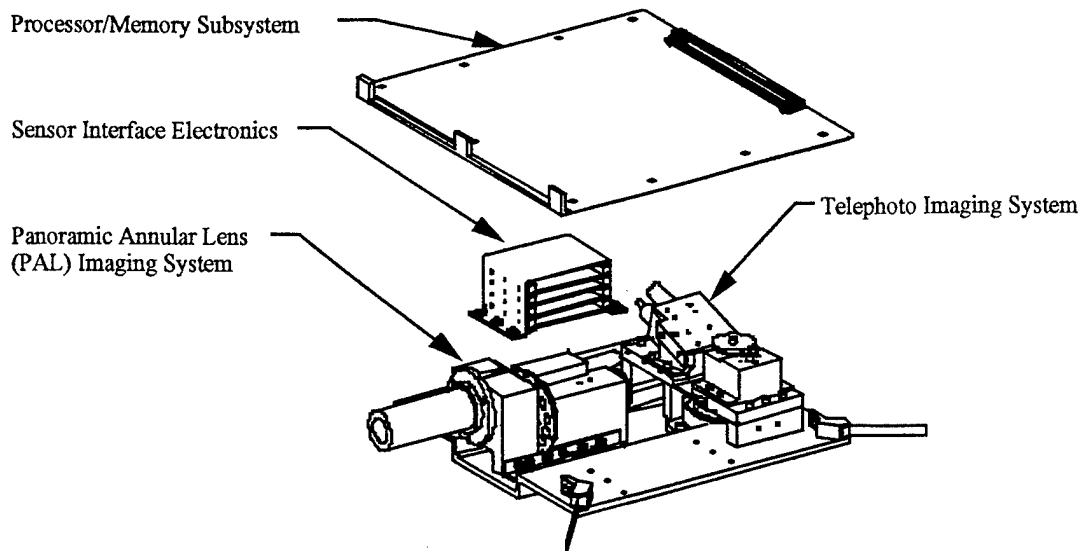


Figure 3.6.1-1 SEASIS Experiment Subsystem

Figure 3.6.1.2 shows a functional block diagram of SEASIS. For both the telephoto system and the PAL system, light is focused by a lens assembly, through a bandpass filter, onto the image plane of a CCD camera. The video digitizer records one image at a time, from either the telephoto camera or PAL camera, digitizes it, and performs a direct memory access (DMA) transfer to the Transputer. The Transputer compresses/processes the digitized image and transfers it to the SEASIS memory subsystem, currently designed for 1 Gigabit of static memory. Images are stored in the memory subsystem until requested by the Command Data System (CDS), the satellite master control system, for down link to earth. The images are transferred by the Transputer from memory, through the processor module, to the CDS. The CDS formats the images for transmission, and then down links the images via a Mode L transponder at 437.85 MHz with a data rate of 9.6, 19.2, 38.5, or 56.0 kbits per second. Two Interpoint DC/DC converters provides power to the experiment from the main satellite power bus. One is for the electronics and the second is for the cameras and stepper motors.

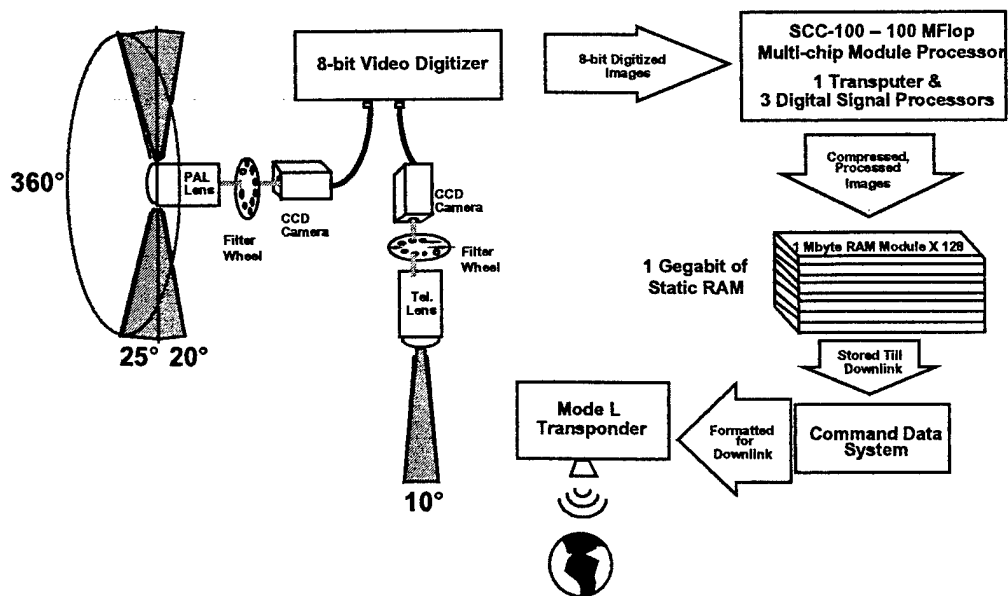
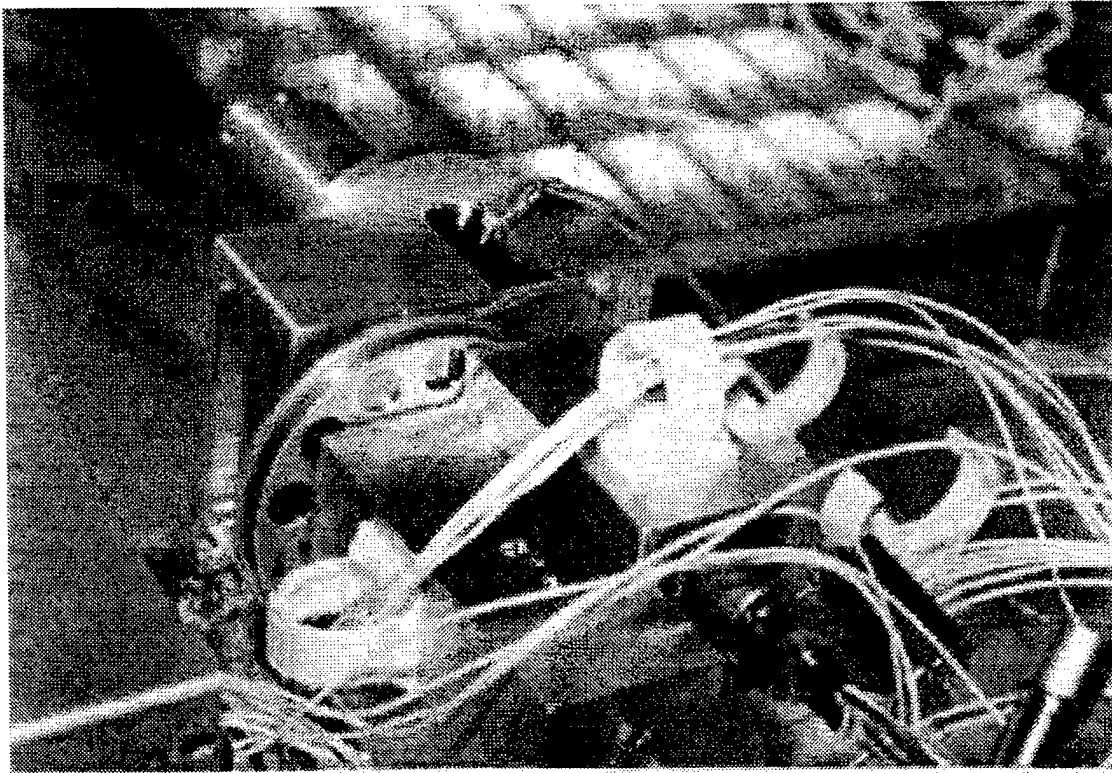


Figure 3.6.1.2 SEASIS Functional Block Diagram



Mission Operations

SEDSAT 1 mission operations commence when the satellite is ejected from the Delta II rocket, separating from the PAF. Separation from the PAF frees the separation switch plungers allowing internal springs to move them to their unloaded position. This closes switches internal to the separation switches, which connect the solar arrays and the battery to the main power bus. There is a 1 second time constant RC circuit that prevents the CDS 80C186 processor from operating during power transients that arise from the abrupt applying of power during switch closure.

After the processor comes out of its reset cycle, it runs through an initialization cycle where the memory is configured by the real time multitasker (kernel). This initialization cycle lasts for approximately 1 second whereupon the kernel begins normal operations by beginning the telemetry capture task which includes recording and processing all telemetry from the power system. The SEASIS system is activated to take images of the receding Delta II second stage. After this task is successfully started, the communications system is initialized and the mode L transponder commanded into its high data rate mode with telemetry, including image data transmitted.

Once ground communications is established new flight software will be uploaded. The onboard software image is limited by constraints of the operating system, but can be readily replaced by software transmitted from the ground.

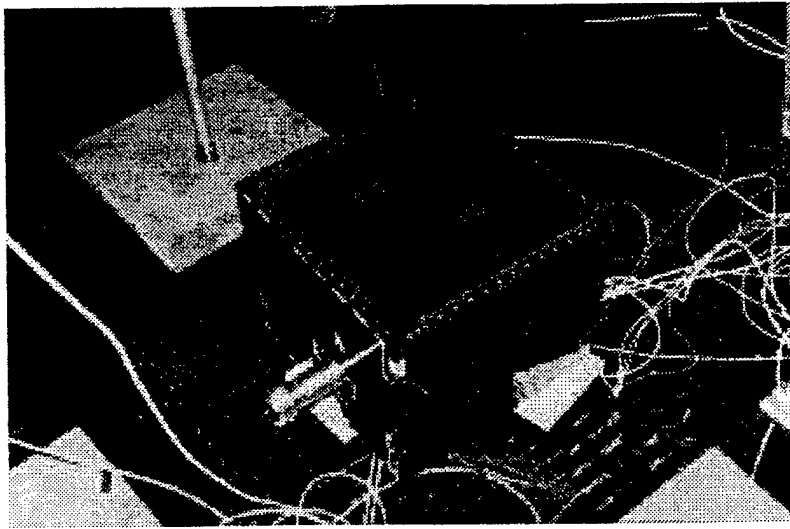
During the mission, the SEDSAT-1 ground team in association with amateur radio organizations will have operational ground stations at many points around the world. A subset of these stations will have Internet connectivity, which will pipeline the data from their radios. This information will be fed to the University of Arizona for retransmission to POCC at NASA JSC, GSFC, MSFC, UAH and to any other Internet site with the appropriate software. The mode A transponder transmit antenna will be deployed after the additional software is uploaded. The post-ejection software upload is required to perform the antenna deployment.

After confirmation of antenna deployment, the satellite will enter a checkout phase prior to engaging as an amateur radio communications satellite and remote sensing platform. At the conclusion of antenna deployment, checkout, and software loading on-orbit operations will commence.

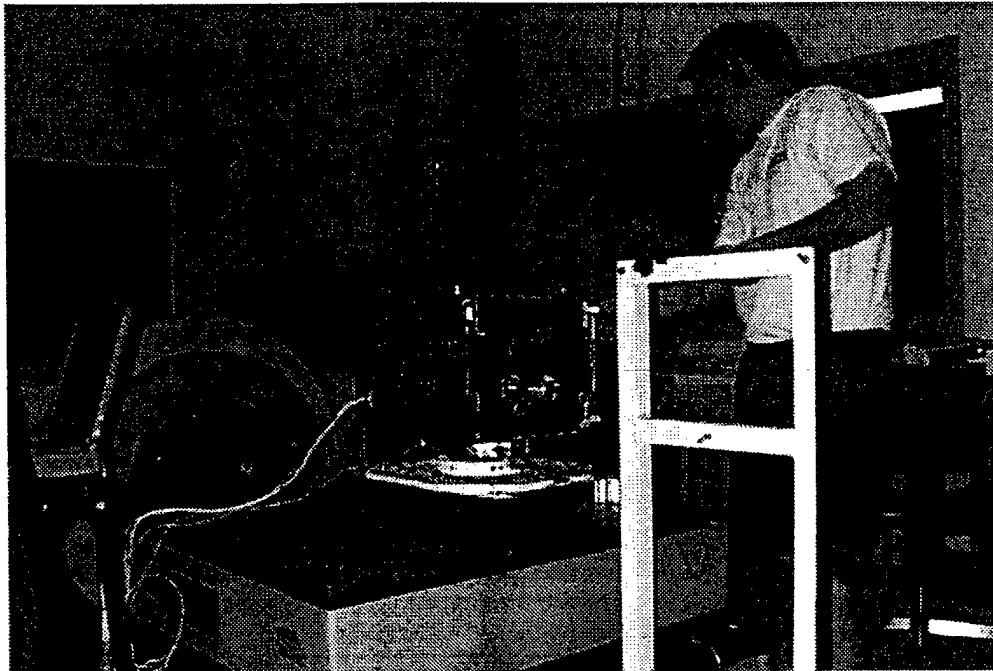
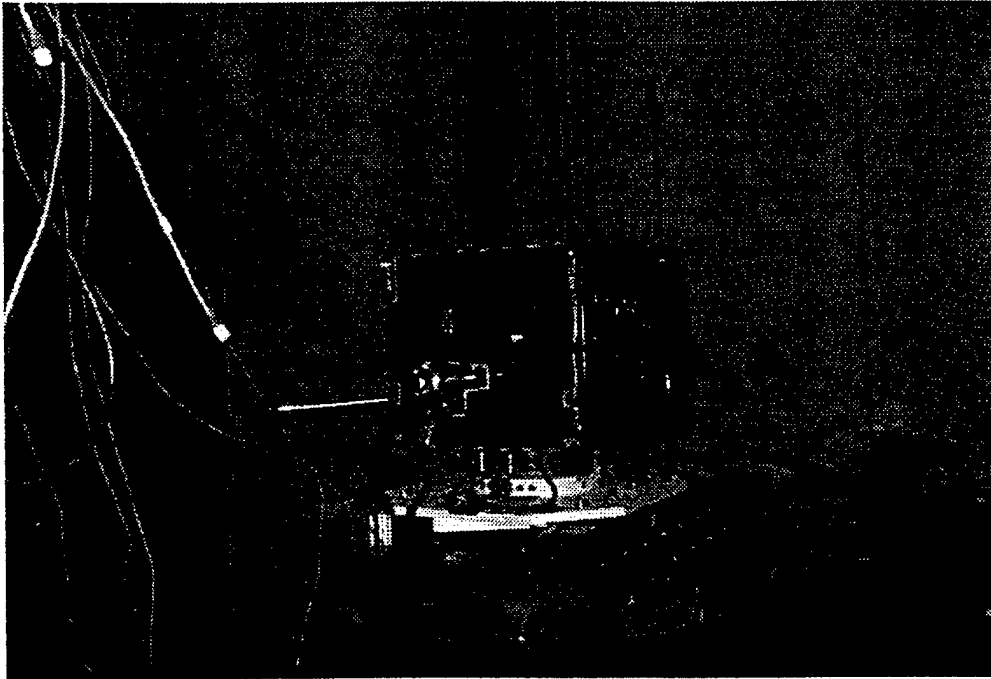
Integration and Test

The SEDSAT qualification and acceptance plan was driven by the Boeing secondary payload requirements as well as engineering needs. Developmental testing was done in the NASA Marshall Space Flight Center thermal-vacuum chamber. Acceptance testing, using proto-flight methodologies and levels, was also performed at NASA Marshall.

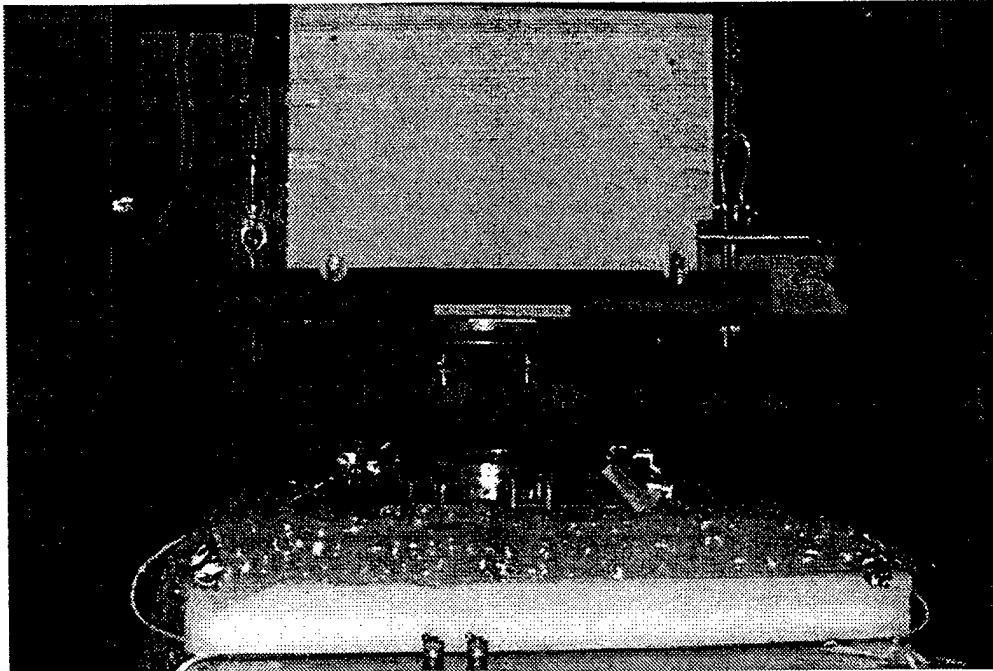
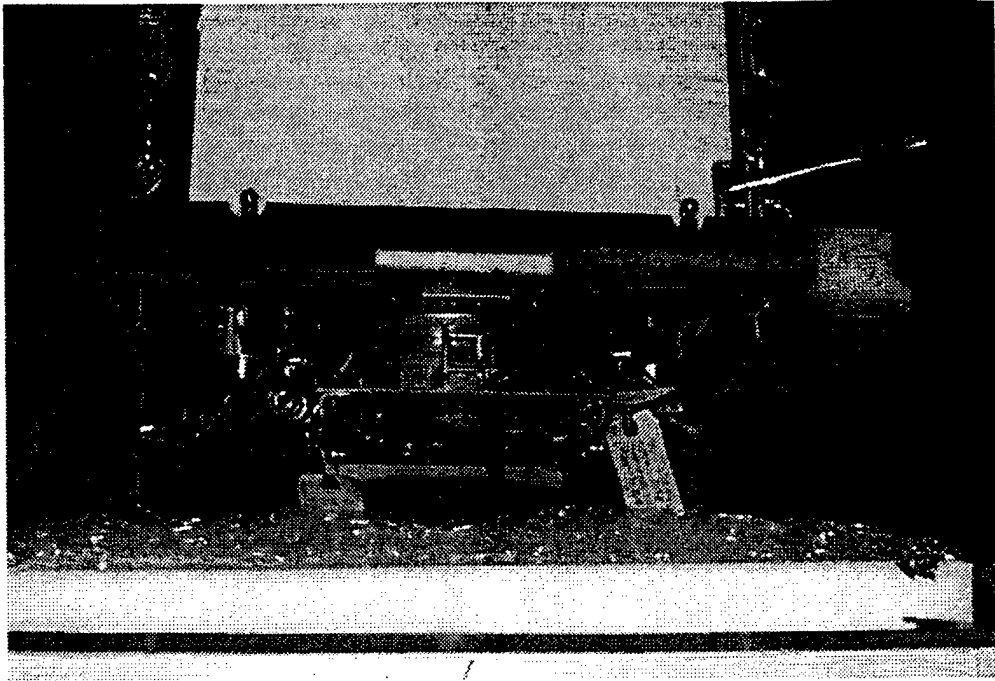
Thermal-Vacuum Test



Vibration Test



Shock Test



Launch Operations

